Planetary and Space Science xxx (2018) 1–18

Contents lists available at ScienceDirect

Planetary and Space Science

journal homepage: www.elsevier.com/locate/pss

Regional unit definition for the nucleus of comet 67P/Churyumov-Gerasimenko on the SHAP7 model

N. Thomas [a,*], M.R. El Maarry [b], P. Theologou [a], F. Preusker [c], F. Scholten [c], L. Jorda [d], S.F. Hviid [c], R. Marschall [a,e], E. Kührt [c], G. Naletto [f,g,h], H. Sierks [i], P.L. Lamy [d], R. Rodrigo [e,j], D. Koschny [k], B. Davidsson [l], M.A. Barucci [m], J.L. Bertaux [n], I. Bertini [o], D. Bodewits [p], G. Cremonese [q], V. Da Deppo [h], S. Debei [r], M. De Cecco [s], S. Fornasier [m], M. Fulle [t], O. Groussin [u], P.J. Gutièrrez [v], C. Güttler [i], W.H. Ip [w,x], H.U. Keller [c,y], J. Knollenberg [c], L.M. Lara [v], M. Lazzarin [o], J.J. Lòpez-Moreno [v], F. Marzari [f], C. Tubiana [i], J.B. Vincent [c]

[a] Physikalisches Institut, Sidlerstr. 5, University of Bern, CH-3012, Bern, Switzerland
[b] Laboratory for Atmospheric and Space Physics, University of Colorado, 3665 Discovery Drive, CO, 80301, USA
[c] Deutsches Zentrum für Luft- und Raumfahrt (DLR), Institut für Planetenforschung, Asteroiden und Kometen, Rutherfordstraße 2, 12489, Berlin, Germany
[d] Laboratoire d'Astrophysique de Marseille, 38 Rue de Frédéric Joliot-Curie, 13388, Marseille, Cedex 13, France
[e] International Space Science Institute, Hallerstraße 6, 3012, Bern, Switzerland
[f] University of Padova, Department of Physics and Astronomy "Galileo Galilei", Via Marzolo 8, 35131, Padova, Italy
[g] University of Padova, Center of Studies and Activities for Space (CISAS) "G. Colombo", Via Venezia 15, 35131, Padova, Italy
[h] CNR-IFN UOS Padova LUXOR, Via Trasea 7, 35131, Padova, Italy
[i] Max Planck Institute for Solar System Research, Justus-von-Liebig-Weg 3, 37077, Göttingen, Germany
[j] Centro de Astrobiologia, CSIC-INTA, 28850, Torrejon de Ardoz, Madrid, Spain
[k] Scientific Support Office, European Space Research and Technology Centre/ESA, Keplerlaan 1, Postbus 299, 2201 AZ Noordwijk ZH, The Netherlands
[l] Jet Propulsion Laboratory, M/S 183-401, 4800 Oak Grove Drive, Pasadena, CA, 91109, USA
[m] LESIA, Observatoire de Paris, Université PSL, CNRS, Univ. Paris Diderot, Sorbonne Paris Cité, Sorbonne Université, 5 place Jules Janssen, 92195, Meudon, France
[n] LATMOS, CNRS/UVSQ/IPSL, 11 Boulevard d'Alembert, 78280, Guyancourt, France
[o] University of Padova, Department of Physics and Astronomy "Galileo Galilei", Vicolo dell'Osservatorio 3, 35122, Padova, Italy
[p] Department of Astronomy, University of Maryland, College Park, MD, 20742-2421, USA
[q] INAF, Astronomical Observatory of Padova, Vicolo dell'Osservatorio 5, 35122, Padova, Italy
[r] University of Padova, Department of Industrial Engineering, Via Venezia 1, 35131, Padova, Italy
[s] University of Trento, Faculty of Engineering, Via Mesiano 77, 38121, Trento, Italy
[t] INAF Astronomical Observatory of Trieste, Via Tiepolo 11, 34143, Trieste, Italy
[u] Aix Marseille Université, CNRS, LAM (Laboratoire d'Astrophysique de Marseille) UMR 7326, 13388, Marseille, France
[v] Instituto de Astrosica de Andalucía (CSIC), c/ Glorieta de la Astronomia s/n, 18008, Granada, Spain
[w] Graduate Institute of Astronomy, National Central University, 300 Chung-Da Rd, Chung-Li, 32054, Taiwan
[x] Space Science Institute, Macau University of Science and Technology, Avenida Wai Long, Taipa, Macau
[y] Institut für Geophysik und extraterrestrische Physik, Technische Universität Braunschweig, Mendelssohnstr. 3, 38106, Braunschweig, Germany

ARTICLE INFO

Keywords:
Rosetta
67P/Churyumov-Gerasimenko
Nucleus
Morphology

ABSTRACT

The previously defined regions on the nucleus of comet 67P/Churyumov-Gerasimenko have been mapped back onto the 3D SHAP7 model of the nucleus (Preusker et al., 2017). The resulting regional definition is therefore self-consistent with boundaries that are well defined in 3 dimensions. The facets belonging to each region are provided as supplementary material. The shape model has then been used to assess inhomogeneity of nucleus surface morphology within individual regions. Several regions show diverse morphology. We propose sub-division of these regions into clearly identifiable units (sub-regions) and a comprehensive table is provided. The surface areas of each sub-region have been computed and statistics based on grouping of unit types are provided. The roughness of each region is also provided in a quantitative manner using a technique derived from computer graphics

* Corresponding author. Physikalisches Institut, Sidlerstrasse 5, University of Bern, 3012, Bern, Switzerland.
E-mail address: nicolas.thomas@space.unibe.ch (N. Thomas).

https://doi.org/10.1016/j.pss.2018.05.019
Received 18 February 2018; Received in revised form 20 April 2018; Accepted 31 May 2018
Available online xxxx

applications. The quantitative method supports the sub-region definition by showing that differences between sub-regions can be numerically justified.

1. Introduction

Observations of the nucleus of 67P/Churyumov-Gerasimenko (hereafter 67P) by the OSIRIS imaging system (Keller et al., 2017) from onboard the European Space Agency's Rosetta spacecraft revealed a bi-lobate object (Sierks et al., 2015) with diverse surface morphology (Thomas et al., 2015a,b). The shape of the nucleus has been refined in several steps (e.g. Preusker et al., 2015, 2017; Jorda et al., 2016) and has now reached metre-scale accuracy over most of the object. 67P can be crudely separated into a roundish "head" representing the smaller lobe of 2.50 km × 2.14 km x 1.64 km (Jorda et al., 2016) and an ellipsoidal "body" representing the larger lobe of 4.10 km × 3.52 km x 1.63 km in dimension. The two lobes are linked by a thin, narrow, "neck" that corresponds to around 7% of the total volume.

The surface morphology was used to define regions in the northern hemisphere by Thomas et al. (2015a,b) and El-Maarry et al. (2015). These regions were intended to group areas with common properties not merely for reasons of nomenclature but also for developing relationships between surface morphology and outgassing properties. This was extended to the southern hemisphere by El-Maarry et al. (2016).

The irregular shape of the nucleus produced significant self-shadowing. This lead to difficulties in tracing regional boundaries in some areas. The neck in the southern hemisphere, for example, could only be observed for a short period because of both the orbit of the comet and the need for Rosetta to remain safe from the effects of reflected light from dust on its star trackers. Hence, some ambiguity arose. Furthermore, analysis of 2D images to produce the boundaries is not simple on such an irregular object. The shape model brings in the third dimension and use of computer tools to view the nucleus from several directions almost simultaneously gives a much clearer vision of the constituent parts of the nucleus. It is also forced to be consistent at boundaries which is something that is not guaranteed when using 2D definitions. We have used this approach to look at the regions individually and thereby identify sub-regions – separating regions where the properties are not uniform across their surfaces.

The approach has been to combine 2D global and local images with the shape model to define sub-regional boundaries. This has also allowed us to look at large dust-covered regions (such as Ash and Ma'at) to obtain a better understanding of the uniformity of the substrate under the dust under the assumption that the dust coverage provided a conformal coating of the surface.

In section 2, we shall look at the regions individually and, using both the shape model and 2D images from OSIRIS, attempt to isolate areas with common properties at approximately the square kilometre scale. In section 3, we shall look at some derived products. We can use the surface areas to define percentage coverage of specific morphologies. The surface roughness in the individual regions can also be calculated to give a more quantitative assessment of the surface morphology. In section 4, we provide some straightforward conclusions.

2. The regional definition

2.1. Regions on SHAP7

The regions on the nucleus of 67P as defined by Thomas et al. (2015a, b) for the northern hemisphere and El-Maarry et al. (2016) for the southern hemisphere are shown in Fig. 1. The montage of 4 different views uses the SHAP7 model of the nucleus (Preusker et al., 2017). The

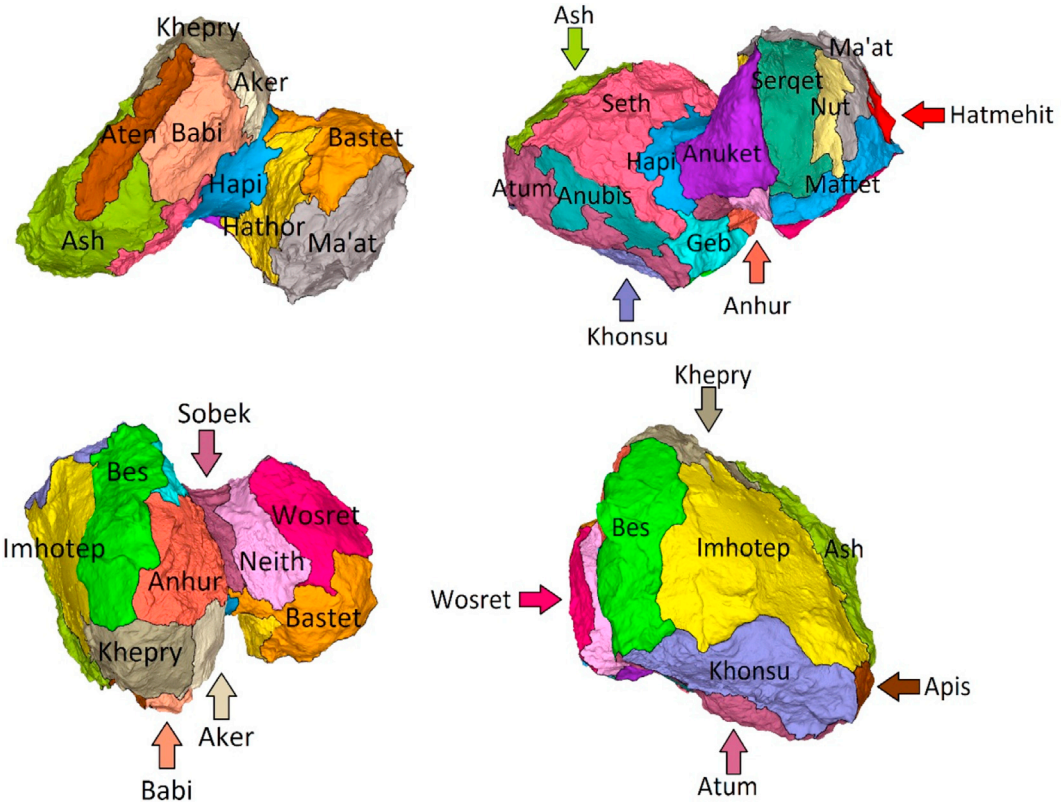

Fig. 1. Montage of 4 orientations of the nucleus of 67P showing the region definitions (Thomas et al., 2015a,b; El-Maarry et al., 2015, 2016) on the SHAP7 model.

Table 1
Each region is sub-divided (where feasible) into sub-regions. The surface area of each region is given and the totals for the head, neck and body regions are also shown. The characteristics of the region and of the sub-regions are given in each case. We also include unique abbreviations for each region to simplify display.

Region	Characteristics and Area [km^2]	
Atum (Am)	Complex region with consolidated material and very rough.	1.9497
	Sub-region a A very rough topographic high (with respect to its surroundings) with boulders and some lineaments.	
	Sub-region b A smooth fractured surface adjoining Khonsu. On the Khonsu side, there is a cliff leading to rough fractured terrains possibly indicating loss of this smooth layer. It is topographically at slightly higher elevation than the adjoining Anubis region with a distinct step evident at the boundary.	
	Sub-region c An undulating terrain with intermediate roughness. It is bounded by Anubis and Anhur on the north and south side respectively and by a steep cliff to the east that forms the Geb region.	
Khonsu (Kn)	Complex region with a mixture of smooth and rough terrains.	2.16872
	Sub-region a This sub-region is at an angle with respect to the rest of the region. It also contains small scale roughness and a lot of boulders.	
	Sub-region b Very rough terrain on many scales adjoining the Apis "face" and showing the side of the rougher part of Atum.	
	Sub-region c Very rough and in places pitted terrain with fractures. Topographically low compared to adjacent Atum sub-regions.	
	Sub-region d Adjoining Atum, this region is very complex. There are flatter areas (dust deposits) but with rough outcrops.	
	Sub-region e A small sub-region which is dominated by flat, apparently dusty material	
Apis (Ap)	Consolidated and fractured but topographically smooth. Topographically stands out above Ash	0.39798
Imhotep (Im)	Smooth "dusty" depression surrounded by more consolidated material. Circular features at the edges of the smooth terrain	4.90446
	Sub-region a Smooth material at the centre of the region. Observed to change dramatically over the mission. Bounded by Ash to the north. On two sides there are steps upwards to rougher terrain (sub-region b) while on the remaining side there are layers downwards to sub-region c with a more gradual transition than elsewhere.	
	Sub-region b Rim of sub-region a. Contains layered terrain incorporating a large circular structure.	
	Sub-region c Rougher terrain inside the rim of Imhotep. Includes all the small quasi-circular structures. Adjoins the smooth terrain. At the boundary there are indications of layering.	
	Sub-region d Clearly rocky at its edge but covered with smooth material in depressions. Evidence of surface changes in places similar to those observed in sub-region a. Boundary to smooth surface (sub-region a) often associated with a clear scarp. Similar to Khepry although topographically lower.	
Anubis (Ab)	Smooth surface probably not consolidated and has undergone surface modification possibly similar to that observed in Imhotep.	0.92241
Bes (Be)	Multiply-layered terrain bordering the scarp into the southern part of the neck.	2.42084
	Sub-region a Topographically lowest level. Covered in boulders in some places.	
	Sub-region b Separated from a by a cliff. Contains a diamond-shaped structure surrounding a surface with large boulders	
	Sub-region c Adjoins Imhotep and appears to be at a level intermediate between sub-regions a and b although it has no contact with a. Generally smooth with no major topographic features.	
	Sub-region d A steep cliff separates this level from sub-region c. It is at a higher topographic level – similar to b or possibly slightly higher.	
	Sub-region e The uppermost level. Separated from d by a significant change in slope. The steep cliff down to Anhur sub-region c is strongly apparent in the shape model.	
Seth (Se)	Consolidated, possibly more brittle in nature when compared to other more strongly consolidated regions. Dominated by circular and semi-circular structures and talus.	4.66022
Ash (As)	Covered with a presumed sedimentary deposit producing smooth surface. Occasional exposures of more consolidated but brittle material below.	6.25734
	Sub-region a Adjoining Babi at an edge and the Aten depression via a sharp change in slope, this sub-region adjoins an adjacent sub-region at a rough hummocky interface. The sub-region is mostly smooth with some smaller depressions and small cliffs covered in dust.	
	Sub-region b Adjoining Seth, this sub-region is smooth. Its boundary to Seth is characterized by a transition to rougher terrain and a substantial change in slope.	
	Sub-region c Adjoining Aten, this is rougher terrain. It is topographically higher than sub-region b and where it meets sub-region b there are arc-shaped cliffs.	
	Sub-region d Dust coated. Smoother region.	
	Sub-region e Sub-region containing the large circular structure which may be the result of impact. Possibly related material outside the putative rim is included.	
	Sub-region f Smooth sub-region with a small pit and some scarps. Intermediate in character.	
	Sub-region g Seth like. Adjoining Atum.	
	Sub-region h Adjoining Apis. Rock-like surface with a slight depression. Topographically separated from the rest.	
	Sub-region i Large-scale rough terrain. Dust covered but with exposed layering in many places. Transitions to the Imhotep region at a boundary between very rough terrain and that of intermediate character.	
	Sub-region j Borders Aten and is also a depression but not as deep as Aten. There is a ridge dividing two sections of the sub-region. The bases of the depression on both sides of the ridge are smooth.	
Aten (An)	Depression with little or no sedimentary deposits. Interior mainly dominated by talus resulting from progressive rim failure.	1.12758
Babi (Bb)	Covered with a deposit producing a smooth surface. Occasional exposures of more consolidated but brittle material below. Topographically separated from Ash.	1.45666
	Sub-region a Topographic high with cliffs on 3 sides. Uppermost surface is dust covered.	
	Sub-region b Topographically low and strongly sloping. Bounded by Khepry, Seth and Ash. Some spur-like structures possibly originating from sub-region a are evident.	
Geb (Gb)	Consolidated material	1.02767
	Sub-region a Large numbers of depressions on a steep slope.	
	Sub-region b The neck side of Geb. Covered in boulders.	
	Sub-region c Smoother fractured surface similar to that seen in Anhur and Bes.	
Khepry (Kp)	Consolidated and fractured material but rather smooth with ponded deposits.	1.63087
	Sub-region a Flat but rocky-like sub-region with ponded deposits	
	Sub-region b A small sub-region with a prominent cliff. Adjoins Bes with similar characteristics.	
	Sub-region c Topographically almost at right-angles to sub-region a. Highly complex sub-region with rough, rocky terrain, smoother coatings it places and boulders. Talus from collapse of material from Ash is also evident.	
Anhur (Ah)	Consolidated material with significant intermediate scale roughness	1.87013
	Sub-region a Plateau with extreme intermediate roughness including isolated ridges. Includes some pits.	
	Sub-region b Cliffs descending from sub-region a to the neck. Surface texture similar to that in sub-region a.	
	Sub-region c With respect to the roughly ellipsoidal shape of the body, topographically on same level as Bes sub-region a which it adjoins but with the face being at a large angle to Bes sub-region a.	

(*continued on next page*)

Table 1 (*continued*)

Region	Characteristics and Area [km^2]	
Aker (Ar)	Strongly consolidated material similar to the adjacent region, Khepry. Contains a large complex fracture system near a steep topographic slope that descends towards Hapi. It has four distinct faces.	0.87022
	Sub-region a Contains a large set of tectonic fractures and a smooth bottomed shallow depression.	
	Sub-region b Topographically distinct from sub-region a but has some similarities. It adjoins Anhur where there is a change is slope and surface roughness.	
	Sub-region c Comprises a cliff that drops sharply to the boundary with Babi at its base. Significant evidence of collapse is evident along the face.	
	Sub-region d Interfaces primarily with Hapi and is a steep fractured cliff.	
TOTAL BODY		31.66
Hapi (Hp)	Smooth, probably non-consolidated surface	1.98356
Sobek (So)	Consolidated material, texturally very rough	0.83735
	Sub-region a Set of quasi-parallel steps/small scarps	
	Sub-region b Boulder-covered terrain	
TOTAL NECK		2.82
Anuket (Ak)	Consolidated, "rocky" appearance. Smooth on large scale but with some large knobs and significant small scale roughness.	2.0523
Neith (Ne)	Mainly comprising the cliff separating Wosret and Sobek. Significant intermediate scale roughness covering the whole region.	1.60746
Maftet (Mf)	Weakly consolidated material dominated by arcuate-shaped depressions and associated talus.	0.67813
Serqet (Sq)	Mix of strongly consolidated material with substantial vertical relief and a smoother dusty deposit area at the base of a cliff.	1.03333
	Sub-region a Vertical fractured cliff adjoining Anuket	
	Sub-region b Flat dust covered surface with ripples possibly of gas driven origin adjoining Nut.	
	Sub-region c Transitional sub-region with rocky material becoming increasingly similar to Maftet-like morphology at the Maftet boundary.	
Nut (Nu)	Depression possibly similar to Aten but significantly shallower.	0.47264
Wosret (Wr)	Consolidated material that appears highly fractured with occasional pits	2.35911
	Sub-region a An apparently flat "face" with ponded materials and knobby textured terrain.	
	Sub-region b Topographically lower than sub-region a and displaying long fracture systems.	
	Sub-region c Rougher terrain with numerous quasi-circular structures and non-aligned ridges and pits.	
Ma'at (Ma)	Covered with a deposit producing a smooth surface on small scales. Occasional exposures of more consolidated but brittle material below. Similar to Ash but with some pits.	3.81651
	Sub-region a Smooth dust-covered shallow depression with knobs	
	Sub-region b Smooth dust-covered shallow depression with knobs and an irregular-shaped ridge-like structure at its centre.	
	Sub-region c Topographically lower with significant numbers of depressions and quasi-circular/arcuate depressions.	
	Sub-region d A plateau at a lower elevation that Ma'at sub-regions around it. Bounds Bastet at a cliff.	
	Sub-region e Large-scale roughness dominated substrate with dust-covering.	
Bastet (Bs)	Consolidated material with texturally rough surface and limited amounts of dust coating.	1.98781
	Sub-region a Smoother terrain adjoining Hatmehit and Wosret.	
	Sub-region b Undulating terrain on a face at an angle with respect to a. Pock-marked in places.	
	Sub-region c Fractured consolidation terrain. Parts of this sub-region show similarity to Hathor which adjoins it.	
Hathor (Hh)	Consolidated, but fractured material on a gravitationally steep slope. Comprises most of the cliff separating Ma'at and Hapi.	2.16217
Hatmehit (Hm)	Large circular depression with a smooth interior (some rocks) surrounded by more consolidated material at the rim.	1.08561
	Sub-region a The floor of the circular depression. This is generally smooth and flat with a small ridge running roughly through the centre. Some talus from fracturing is evident at the margins.	
	Sub-region b The south and west sides of the rim of the depression adjoining Maftet and Wosret. Contains quasi-circular depressions. The rim of Hatmehit is less pronounced.	
	Sub-region c The north and east sides of the rim of Hatmehit adjoining Bastet and Maat. The steepest parts of the rim are included in this sub-region. The interior of the rim is fractured in many places.	
TOTAL HEAD		17.26

previous works used 2D imaging of the nucleus to support the determination of topographical and morphological boundaries. These were transposed onto the 3D shape model to produce Fig. 1.

A key aspect of this work is whether an independent person would reach similar conclusions in defining unit boundaries. Using the 3D model, there are three boundaries on 67P where an improved definition could be foreseen.

The area around the interfaces between Hapi, Sobek, Neith, Hathor, and Bastet is a good example. In this area, the neck is narrow between Aker on the body side and Bastet/Hathor on the head side. Hapi is smooth and dust covered whereas Aker is rocky in appearance but also relatively smooth. The difficulty arises from where the rough terrain of Sobek and Neith meets the rough terrain of Bastet and Hathor. The extent to which a common unit extends into the neck is uncertain.

The 3D shape model suggests an alternative interpretation of the boundary between Geb, Bes, and Anhur. It can be seen in 3D that part of Anhur extends upwards onto a plateau that could be defined as part of Bes. This suggests that this sub-region was originally misclassified because of the lack of observations and a detailed shape model in 2015. We shall address this below in defining sub-regions.

Finally, the Khepry region has two major components that are almost orthogonal to each other when mapped onto the shape model. This is potentially misleading and could be re-defined. Again, we address this below in defining sub-regions.

Our philosophy throughout is to maintain the previous nomenclature as the number of possible misclassifications is rather small but to identify possible reclassification by using the sub-region definition.

The full sub-region definition is provided in the form of a table (Table 1) and provides 71 separate sub-regions. We refer to this sub-region nomenclature in this table throughout.

2.2. Regions and evidence of internal units

2.2.1. Body

2.2.1.1. Atum (Am) and Anubis (Ab). Atum is a complex region that was close to the terminator in most images during the early phase of the mission. It can now be seen to have 3 distinct sub-regions. The largest sub-region (sub-region a in grey in Fig. 2 left) is a very rough, topographically high, structure bounded by Anubis to the north (pink) and Khonsu to the south (violet). The cliff down to Khonsu is steep. The border with Anubis is gradual.

In the regional definition, this sub-region was originally linked to further rough terrain (light pink in Fig. 2 right) via a thin "bridge". It can be seen in Fig. 2 left that the bridge (cream coloured in Fig. 2) is smooth but topographically slightly higher than the Anubis plains material. High resolution data show it to be fractured. There is a steep cliff downwards to Khonsu on the south side. For the sub-region definition, the cream region is referred to Atum sub-region b. The remaining terrain is undulating with intermediate roughness. This is sub-region c.

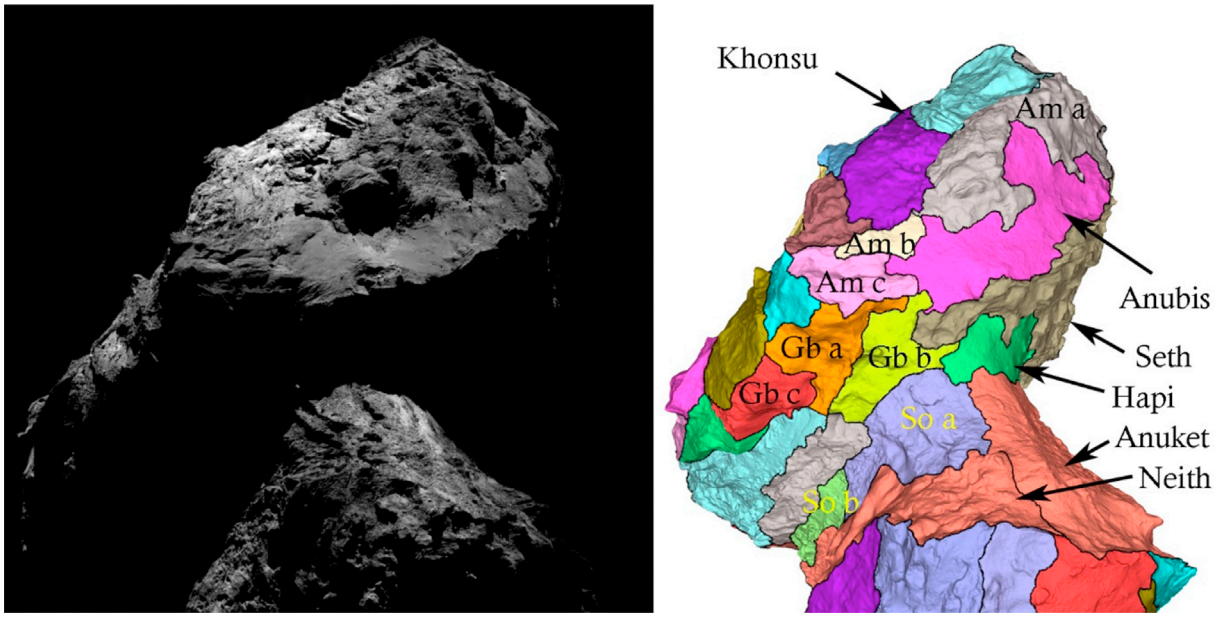

Fig. 2. Left: OSIRIS image (NAC_2015-12-10T05.01.06.778Z_ID10_1397549000_F22) showing the Anubis-Atum-Khonsu face on the body and the Anuket-Neith-Sobek section on the head. Right: The regional definition on the shape model with sub-regions added in the same orientation as the image.

There appear to be no large variations in morphology across Anubis and hence there are no sub-regions defined. The region showed some surface changes during the mission (El-Maarry et al., 2017a,b) akin to scarp retreats. The changes appeared to be similar to those seen in the smooth central part of Imhotep and some parts of Hapi (quasi-circular depressions forming in smooth terrain).

2.2.1.2. Khonsu (Kn) and Apis (Ap). The Khonsu region was first defined after equinox and is a highly complex region with significant evidence of surface changes probably produced by activity (El-Maarry et al., 2017a, b). Changes in surface morphology over small scales are evident. A highly detailed definition would result in a large number of sub-regions. Here, we restrict the definition to 5 main sub-regions.

Sub-region a (Fig. 3 light blue) is inclined with respect to the rest of the region although the change in orientation is smooth and not cliff-like. This is evident in Fig. 3 left from the change in reflectance. It also contains small scale roughness and a lot of boulders. It is bounded by the Imhotep region close to the large quasi-circular structure (yellow in Fig. 3 right).

Sub-region b is very rough terrain on many scales. It adjoins the Apis "face" (green in Fig. 3 right) and has a very sharp boundary defined by the top of a cliff. The north boundary is defined by Atum (sub-region a). The terrain here is probably related to the material making up the elevated topography of Atum. This rougher terrain is evident in Fig. 3 left and there is a change in reflectance within the Khonsu region indicating an internal sub-region boundary.

Sub-region d is bounded by Atum to the north. It is possibly the most complex sub-region on the nucleus with highly varied terrain types

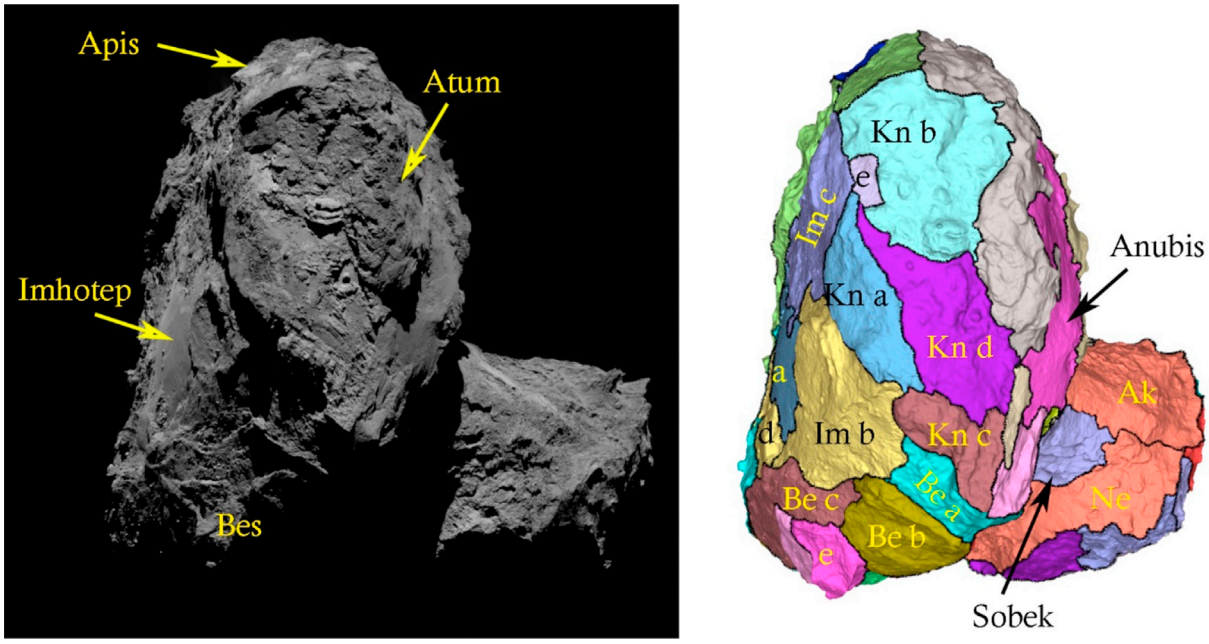

Fig. 3. Left: The Khonsu face of the nucleus (NAC_2015-05-02T15.09.20.389Z_ID10_1397549000_F23). Right: The sub-region definition of Khonsu.

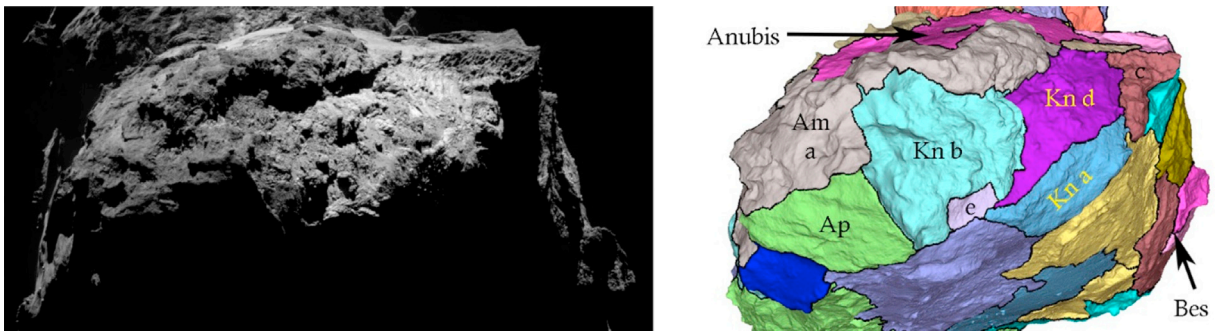

Fig. 4. Left: OSIRIS image (NAC_2015-12-18T03.43.20) showing the Khonsu region and its relationship to Atum (particularly sub-region a) and Apis.

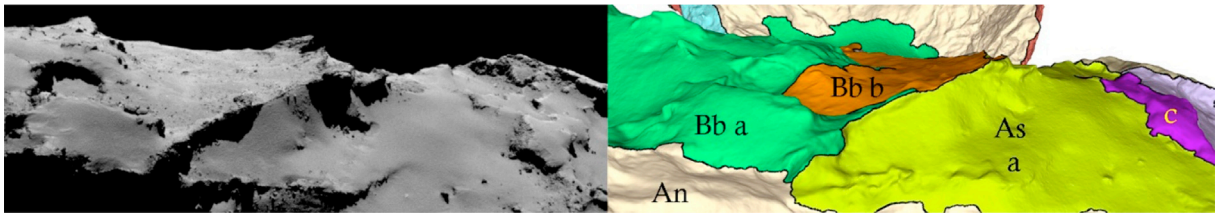

Fig. 5. Left: OSIRIS image NAC_2014-12-02T07.59.13.739Z_ID10_1397549001_F23 showing the edge defining the interface between Ash and Babi. The shape model (right) shows sub-region a in yellow. The hummocky interface to sub-region c (purple) is also visible. (For interpretation of the references to colour in this figure legend, the reader is referred to the Web version of this article.)

(smooth, boulder covered, aligned lineaments etc.). It is deserving of a detailed sub-regional mapping which is unfortunately beyond the scope here. It has shown evidence of significant surface changes during the monitoring of the nucleus including motion of decametre-scale boulders. The boundary with Atum sub-region a is clearly defined by the edge of the rougher Atum material. The boundary with Atum sub-region b is also well defined by the small cliff and the change in surface texture. However, there is also a change in texture between this sub-region and the steep cliff that defines the Khonsu boundary with Bes. The sub-region is significantly rougher in appearance. Fig. 4 shows the roughness of the cliff leading up to Atum sub-regions b and c. The right hand-side of the cliff is both higher and rougher. We define this as sub-region c and it is indicated in brown in the 3D shape model maps.

A small smooth area can be distinguished between sub-regions a and b which we refer to as sub-region e.

2.2.1.3. Ash (As) and Aten (An). The Ash region on the body of the nucleus was defined as being an area covering much of the northern hemisphere and covered in a dust deposit that was assumed to be the result of sedimentation of non-escaping particles returning to the nucleus. The adjacent Babi region was not well observed during the first months of the mission. In particular, the surface towards Aker was ill-defined. The latest shape model has improved the definition of the interface to Aker markedly.

Ash is covered with dust but at $>6\,km^2$, it is the largest region in the nucleus definition. The small scale surface texture provides almost no

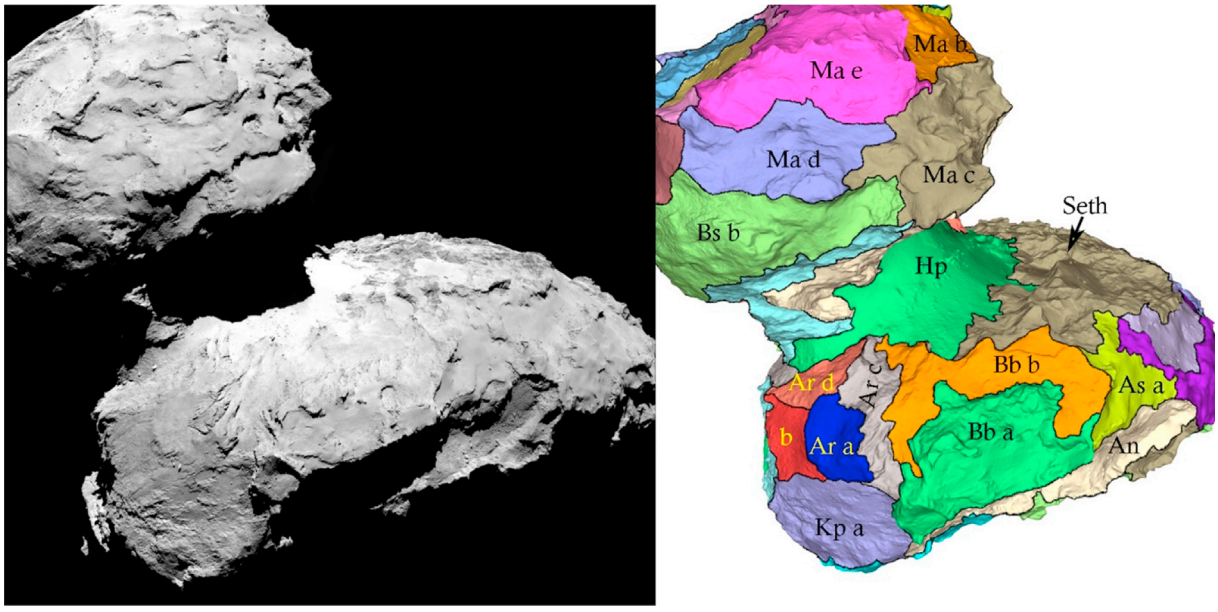

Fig. 6. Left: OSIRIS image NAC_2014-08-16T18.59.14. Right: The corresponding sub-region definition. Note the positions of the Aker sub-regions and their relationship to the two sub-regions of Babi. Note also the sub-regions of Ash.

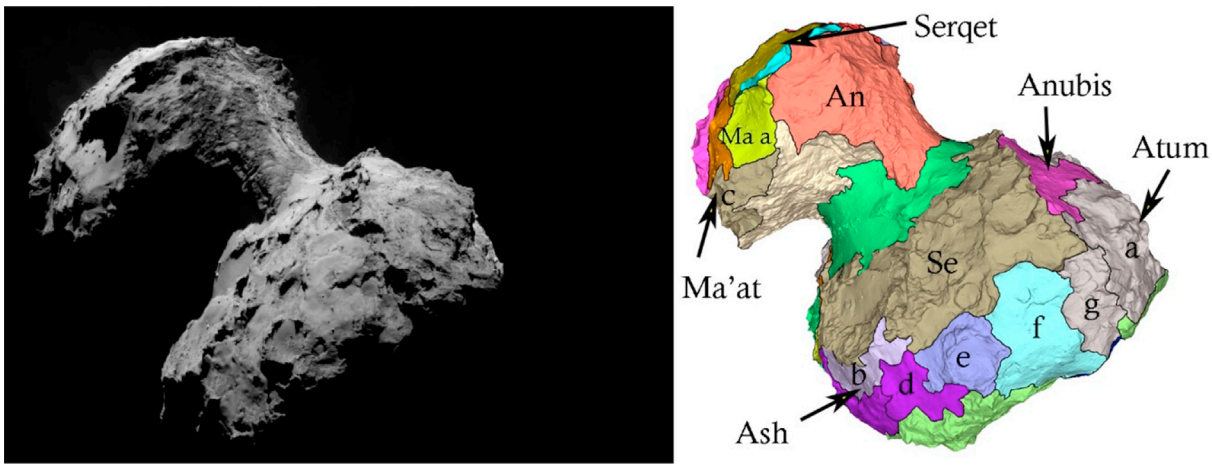

Fig. 7. Left: OSIRIS image NAC_2015-05-11T20.29.18 Right: The sub-region definition. Note the circular structure defined as Ash sub-region e and the Seth-like part of Ash, sub-region g.

assistance in defining sub-regions because of the dust coverage. Hence, we have used the shape model to look in detail at the topography and what can be seen of the substrate. In general, depressions have been isolated and cliffs or sharp changes in slope used to define boundaries. This has resulted in 10 different sub-regions (see also Fig. 7).

The interface to Babi is well defined by a topographic edge (Fig. 5). Adjoining Babi at an edge and the Aten depression via a sharp change in slope, sub-region a adjoins an adjacent sub-region at a rough hummocky interface. The sub-region is mostly smooth with some smaller depressions and small cliffs covered in dust.

Sub-region b is bordered on one side by Seth (Fig. 6). This sub-region is smooth. Its boundary to Seth is characterized by a transition to rougher terrain and a substantial change in slope. It is surrounded on two sides by sub-region c. The boundary with Seth is near the largest flat structure (Aswan) in that region.

Adjoining Aten, sub-region c has rougher terrain. It is topographically higher than sub-region b and where it meets sub-region b there are arc-shaped cliffs. The cliffs are dust-covered.

Sub-region d is adjacent to sub-regions b and c. It is smooth and sits in a depression between a putative impact structure, the highly complex, very rough and extensive sub-region h, and the rougher terrain of sub-region b. The circular structure which is possibly of impact origin and what appears to be related material is defined as sub-region e (Fig. 7). Sub-region d appears rather similar to sub-region b.

Sub-region f is mostly smooth with one significant irregular pit. It is bounded in the direction towards Atum by sub-region g. The boundary here is defined by cliffs. Sub-region g contains several quasi-circular depressions and is therefore similar to Seth which it bounds on one of its short sides. Sub-region g is topographically low compared to its surroundings but is bounded by a sharp change in slope at the interface to sub-region h.

Sub-region h is bounded by a planar surface with elevated topography (Apis) on one side and by the start of the Imhotep depression on another (Fig. 8). The boundary to Ash sub-regions f and g is characterized by a sharp edge and a change in slope. The boundary to sub-region i is also characterized by an edge. Sub-region h has small scale roughness but limited larger scale roughness.

Sub-region i has major large-scale roughness with significant evidence of layering in cliffs. Sub-region j (Fig. 9) borders Aten and is also a depression but not as deep as Aten. There is a ridge dividing two sections

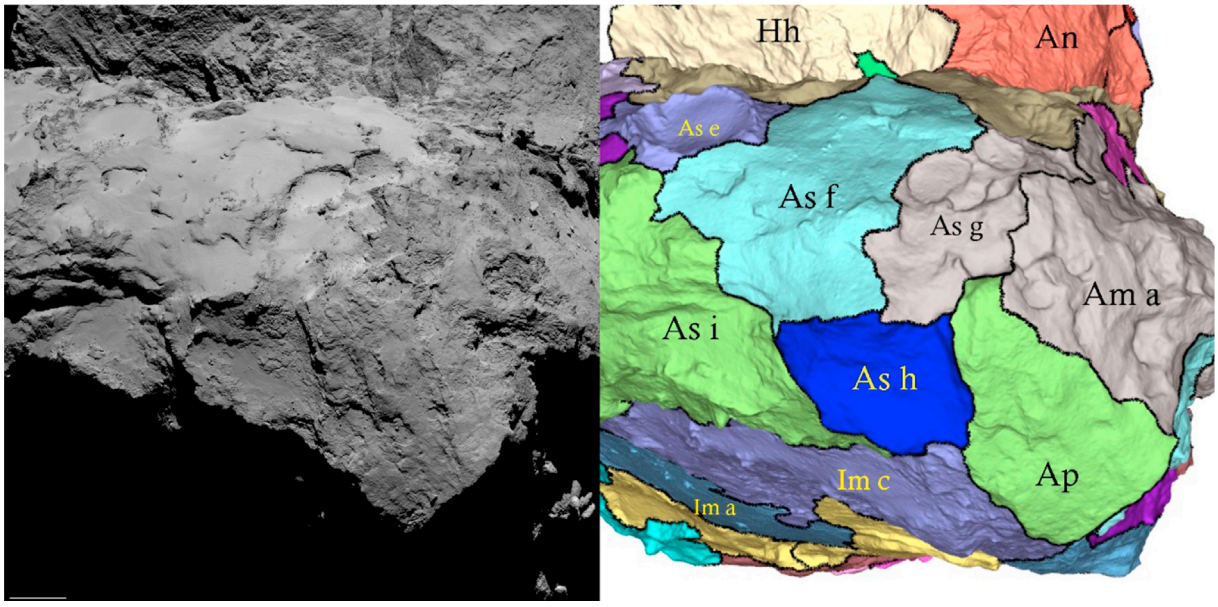

Fig. 8. Left: OSIRIS image NAC_2014-09-02T12.44.22. Right: The sub-region definition. Apis and Atum show much reduced dust-coverage compared to Ash while the Ash sub-regions show different topography. Note the presence of layering in sub-region i.

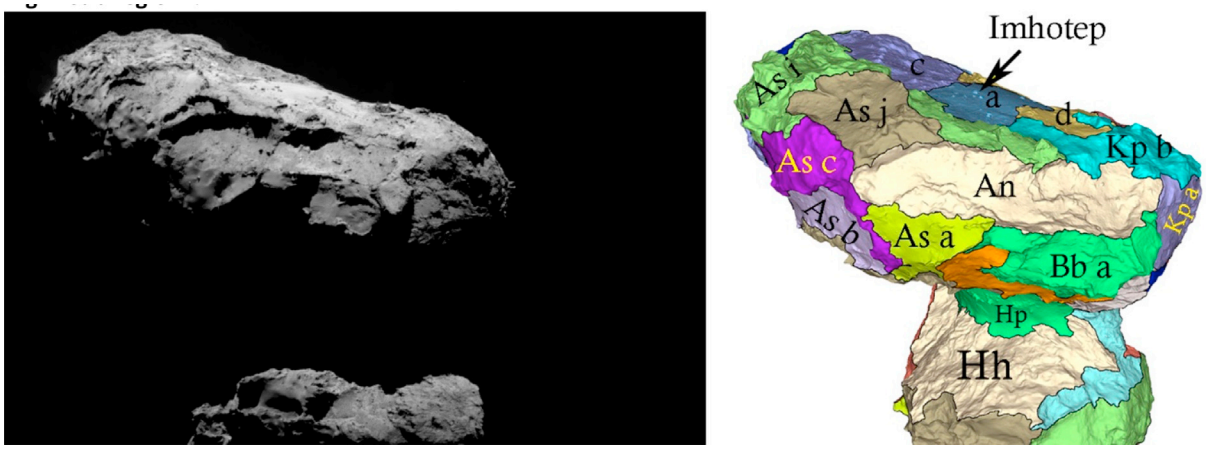

Fig. 9. Left: OSIRIS image NAC_2015-05-11T13.07.42. Right: The sub-region definition showing Aten at the centre of the body in this view. Note the brown coloured sub-region (Ash j) which is a dust-covered depression (but much shallower than Aten). (For interpretation of the references to colour in this figure legend, the reader is referred to the Web version of this article.)

of the sub-region. The bases of the depression on both sides of the ridge are smooth.

There appears to be little reason to sub-divide Aten. The depression structure and its interior are well-defined and there do not seem to be any significant changes or boundaries within it.

2.2.1.4. Aker (Ar), Babi (Bb), and Khepry (Kp). Aker is a highly unusual region (Fig. 10). It has been split into four sub-regions reflecting four distinct faces of the surface in this region. Sub-regions a and b could be clearly seen in the early phase of the mission. Sub-region a is defined to contain the long (>200 m) tectonic fractures that were identified (Thomas et al., 2015a,b). It is separated from sub-region b by a ridge. The boundary here is not extremely sharp but evident in images with low solar incidence. The basic appearance of the surfaces of these two sub-regions is very similar.

The early images gave poor coverage of the surfaces towards Hapi and towards Babi. Both are now shown to be steep cliffs associated with sharp changes in slope. They lead to Aker having an almost cube-like appearance. Sub-region c adjoins Babi and is characterized by a steep cliff with evidence of mass wasting (collapse). The face is not as regular as sub-region d. Sub-region d is a relative flat face leading straight down to the Hapi region in the neck (Fig. 10).

Fig. 6 also shows that Babi has been split in to two sub-regions characterized by very different large-scale surface roughness. The rougher sub-region, a, is dust covered on its northern facing surfaces but there are numerous quasi-circular structures and cliffs. The smoother sub-region, b, passes from the boundary with Ash below the cliffs to the interface (also a cliff) with Aker sub-region c. Most of the surface between Babi sub-region a and the Aker region is topographically low and has not been well-observed because it is surrounded on 3 sides by higher relief.

The Khepry region extends from Aker to Imhotep and is bounded by Babi and Aten on one side and Anhur on the other. The sub-region closest to Aker, sub-region a, is a flat but rock-like sub-region with ponded deposits. Sub-region c is topographically almost at right-angles to sub-region a and close to being in the same plane as most of the Imhotep region. It is a highly complex sub-region with rough, rocky terrain, smoother coatings in places and boulders. Talus from collapse of material from Ash is also evident. A small sub-region with a prominent cliff is defined as sub-region b. This adjoins Bes and is very similar to it. An alternative classification might assign this sub-region to the Bes region.

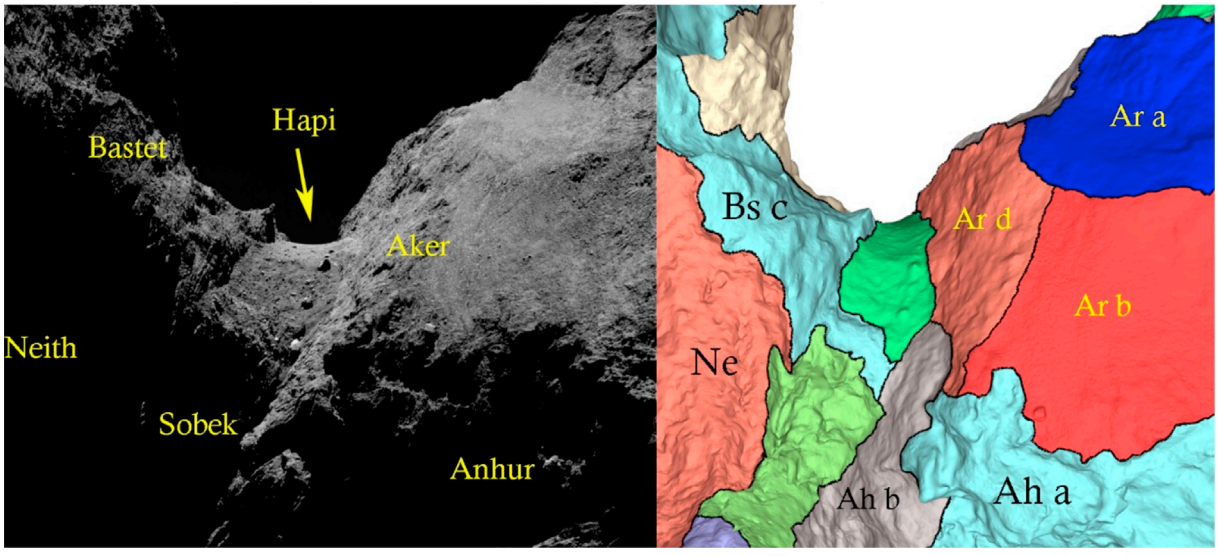

Fig. 10. Left: OSIRIS image NAC_2014-11-22T10.52.53.805Z_ID10_1397549000_F22. Right: The sub-region definition showing in particular the face of Aker leading down to the Hapi region in the neck.

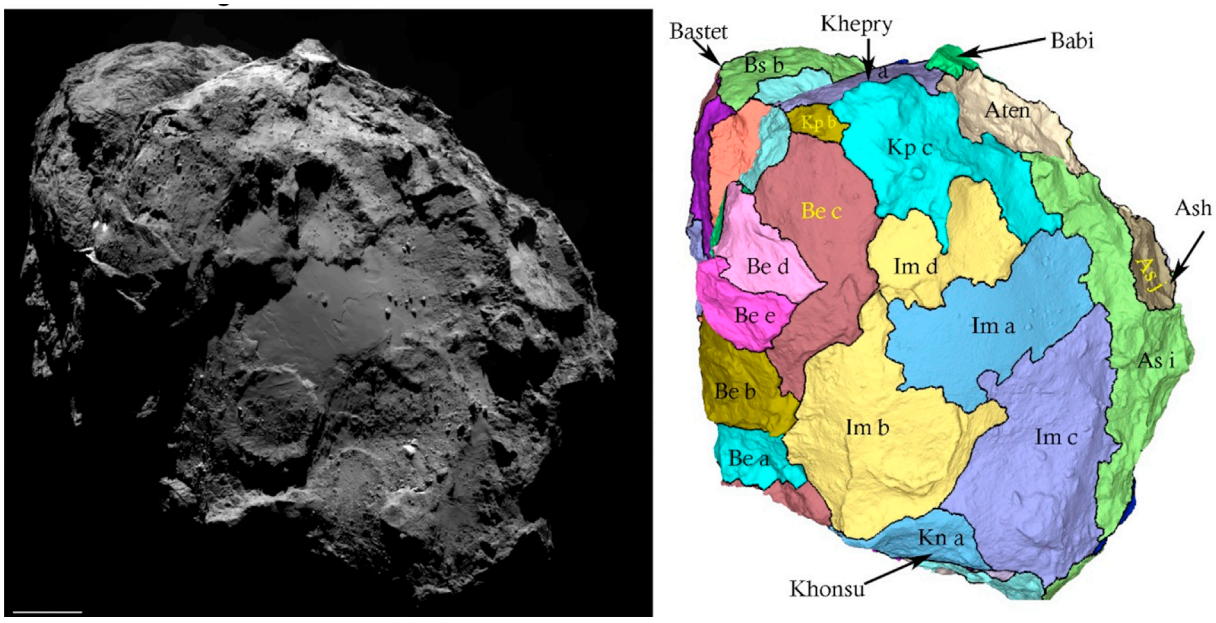

Fig. 11. Left: OSIRIS image NAC_2015-04-29T17.24.09. Right: The sub-region definition for Imhotep.

2.2.1.5. Imhotep (Im). Imhotep is one of the most striking regions on 67P and was originally defined through being a large depression with its surroundings being at higher elevation. The texture of the surface in its interior is however remarkably diverse and we use this diversity to identify 4 sub-regions.

Sub-region a is the smooth terrain at the centre of Imhotep (Fig. 11). It contains just a few boulders and shows surface features that changed throughout the mission. Sub-region b is at a notably higher elevation. It appears to be dust-covered in most places but is appreciably rougher in small-scale surface texture. It also encompasses a large, dust-filled, circular structure with layering. Sub-region c is rough on intermediate scales and contains the small circular structures that might be connected to similar features seen on Tempel 1. At the interface to sub-region a, there are layers that seem to have been exposed by some form of mass wasting and sub-region c, at its border with sub-region a, is at a significantly lower elevation. However, there are other structures within sub-region c that are at higher elevation.

Fig. 12 shows an image taken from rotating the shape model to a specific orientation and illustrates the different surface types within Imhotep and the topographical relationships between them. The topographical changes between Imhotep, Ash and Apis are well seen in this view as well.

2.2.1.6. Anhur (Ah), Geb (Gb) and Bes (Be). Anhur is of extreme intermediate-scale roughness and in the southern hemisphere. It bounds Aker and Khepry and extends down into the neck while being bounded elsewhere by Geb and Bes. The improved shape model shows that Anhur has three distinct parts (Fig. 13). The intermediate roughness area

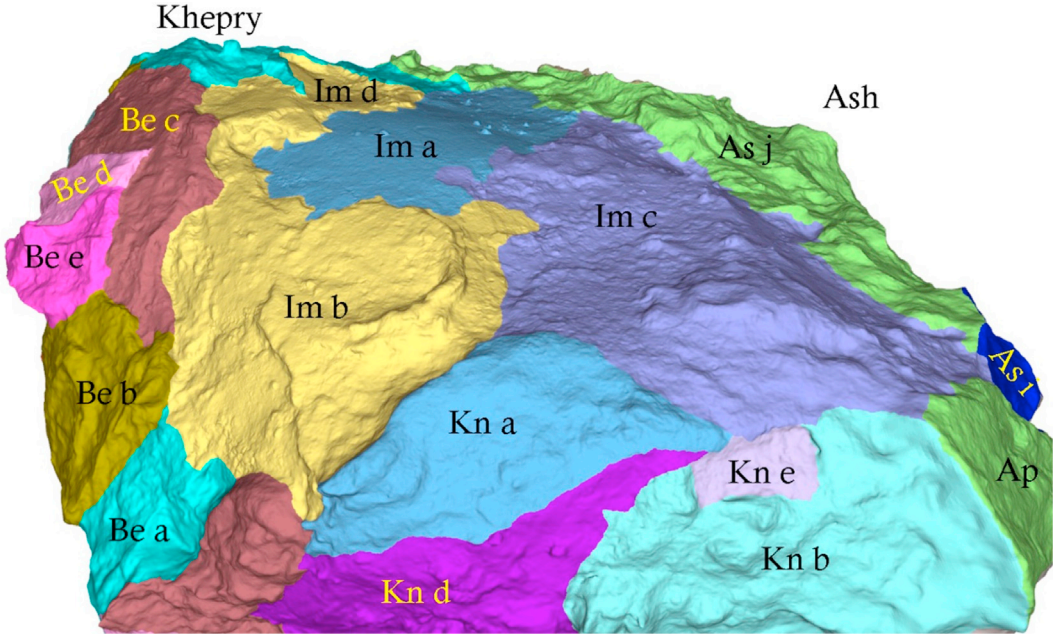

Fig. 12. View of the 3D shape model which emphasizes the topographic differences within the Imhotep region. The relationships of Imhotep (sub-regions a-c) to Ash and Apis are also well brought out in this view. The Bes sub-regions (a–e) are also evident on the left of the diagram. Two sub-regions (i and j) of Ash are marked.

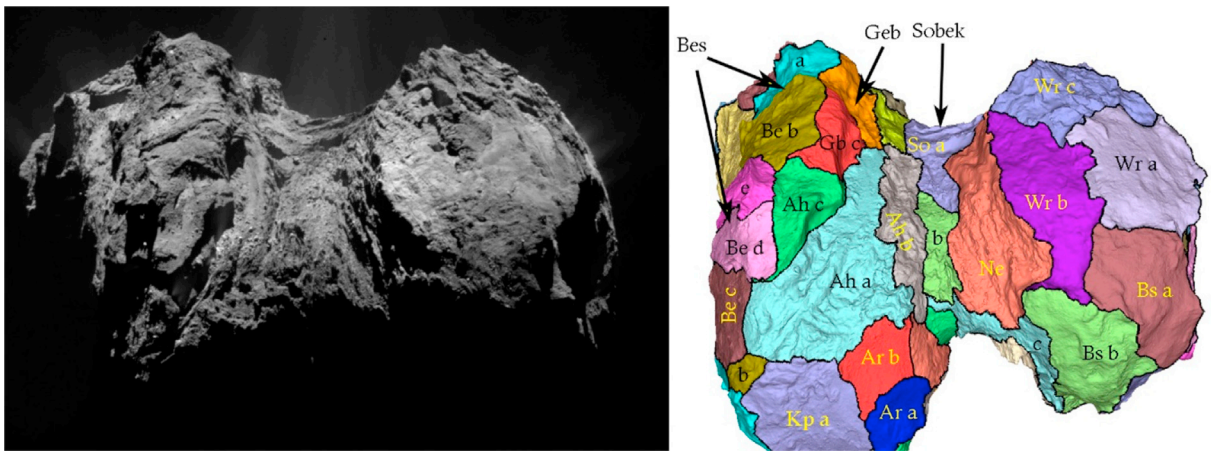

Fig. 13. Left: OSIRIS image NAC_2015-08-01T13.51.57. Right: The sub-region definition. Anhur sub-region a (light blue) is bounded by the cliff (Anhur sub-region b) that descends into the neck. Note that Anhur sub-region c (green) has similar topographical properties to the Geb region. (For interpretation of the references to colour in this figure legend, the reader is referred to the Web version of this article.)

adjacent to Aker and Khepry forms sub-region a. It is mostly a plateau with ridges and some pits. Sub-region b is almost orthogonal to it. The sub-region b cliffs are steep and form the transition from the body to the neck.

Sub-region c is similar to the Bes region. It contains a cliff and a plateau. The topographical relationship to Bes and Geb is also evident when the shape model is manipulated to a specific view (Fig. 14).

The boundaries between Anhur sub-region c, Geb and Bes illustrate the importance of the shape model. The original southern hemisphere definition needed to be performed before the shape model for the southern hemisphere was available. Having only a limited number of 2D images from vertically above the area also reduced the topographic contrast and limited our understanding of the topographic relationships. It is apparent here however that sub-region c of Anhur is most closely related (structurally and textural) to Bes and Geb as previously pointed out by Fornasier et al., (2017).

Geb has been separated into 3 sub-regions. Sub-region b is similar to Anhur sub-region b. It is a cliff dropping down to the bottom of the neck where it meets Sobek. The cliff is not quite as steep as in Anhur and the surface is a little smoother. Sub-region c is the interface to Anhur sub-region c and to the Bes region. It mostly comprises a steep cliff and the area close to its upper edge. The boundary to Bes at this point is gradual and some uncertainty in the exact positioning is evident.

The most interesting element of Geb is sub-region a. This is also cliff-like but here the cliff is highly fractured with numerous pits. Its surface appearance is most similar to areas in Wosret – on the head of the nucleus (Fig. 15) and distinguishes it clearly from other sub-regions in the vicinity.

Bes region has 5 sub-regions that are topographically distinct (Fig. 16). This is most obvious when the region is viewed obliquely from the direction of Khonsu and Atum. There are mostly clearly defined step/cliffs leading from one topographic layer to another. The lowest level (sub-region a) abuts Atum sub-region c and the Khonsu region. It is rough and strewn with boulders. One side adjoins Imhotep. Here, the surface

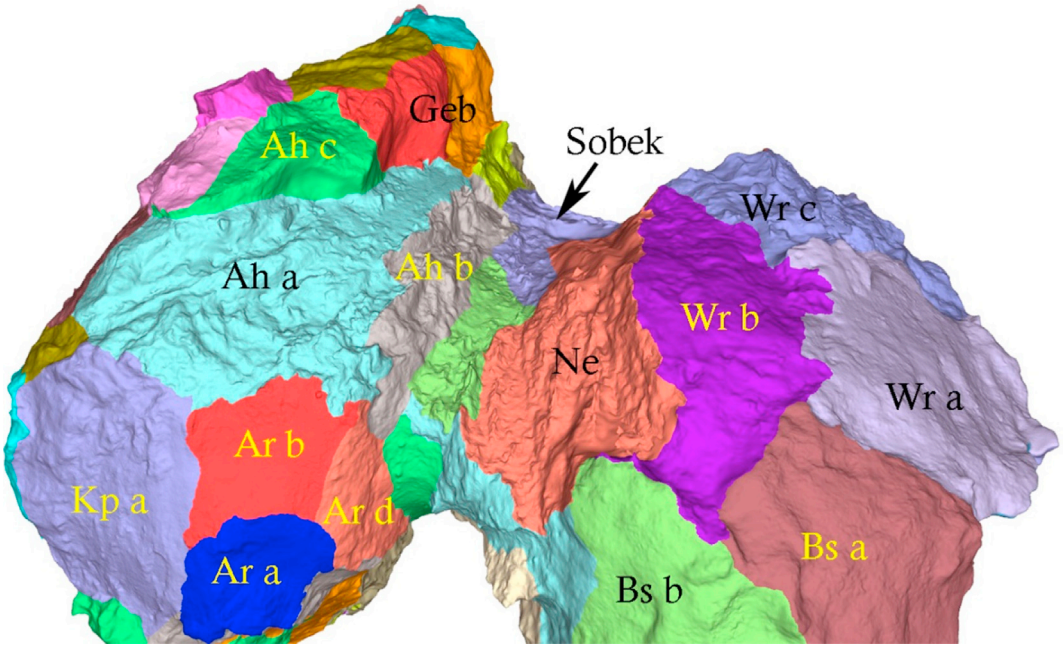

Fig. 14. The shape model oriented to show clearly the topographic relationships between the different sub-regions of Anhur and the Geb region. The topographical relations within Wosret are also well-seen in this view. Other major sub-regions are marked.

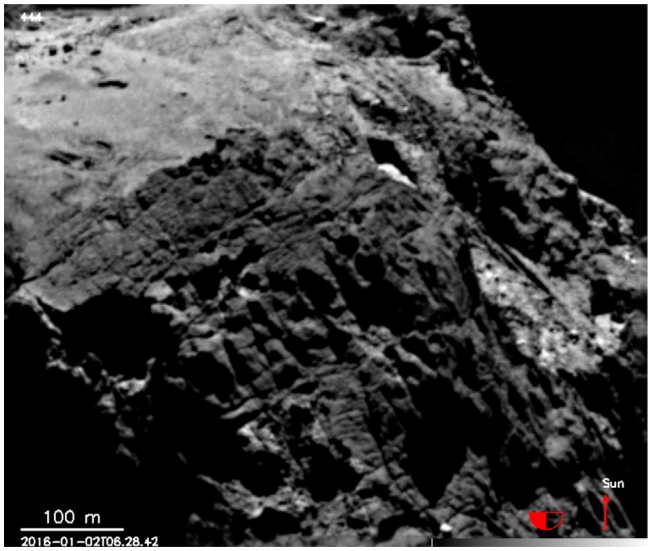

Fig. 15. OSIRIS image acquired on 2 Jan 2016 at 06:28:42 showing sub-region a of Geb. The flat, smooth region above it is Anubis. The cliff of Geb is highly fractured and pitted.

drops but not steeply into the Imhotep region. A cliff forms the border with sub-region b of Bes.

The surface of sub-region b has boulders and a roughly diamond shaped set of ridges. Sub-region c is reached via a small step downwards. Sub-region c is topographically higher than Imhotep (which it abuts) and is separated from it by a cliff. Sub-region c is quite smooth at intermediate and large scales.

A steep cliff separates sub-region d from sub-region c. It is at a higher topographic level and probably higher than that of b. The top surface has boulders. Evidence of collapse of the cliff material on sub-region c is present and blurs the exact definition of the base of the cliff. The uppermost level is sub-region e. It is separated from d by a significant change in slope. The steep cliff down to Anhur sub-region c is strongly apparent in the shape model.

The entire region gives the impression of distinct layers delineated by steep cliffs.

2.2.1.7. Seth (Se) and Anubis (Ab). Seth and Anubis are both larger areas in the shape model. Seth, for example, covers 4.66 km^2. However, the regional definition seems robust in both cases and there seems to be no requirement to sub-divide these regions. The remarkable active pits (Vincent et al., 2016) and semi-circular depressions (Ip et al., 2016) cover the entire Seth region. Anubis, on the other hand, has a very smooth terrain. The boundary with Atum is gradual but the other sides are well-defined by topography and the internal structure is smooth with some boulders. If further sub-division of Anubis into units is performed in future, care must be taken with assessing surface changes as these were significant in Anubis during the mission.

2.2.2. Neck

2.2.2.1. Hapi (Hp). The neck of the nucleus in the northern hemisphere is dominated by the smooth terrain mapped by Thomas et al. (2015a,b) and called Hapi. Here there is little reason to modify or sub-divide this region. There are subtle exposures of more consolidated material in some places but these are very limited in extent.

2.2.2.2. Sobek (So) and Neith (Ne). The neck in the southern hemisphere is considerably more complex texturally than in the north. Furthermore, there are some local areas where the shape model has a lower quality because of the absence of good quality images with adequate illumination. This particularly influences the Neith region. Neith is bounded by Wosret on one side and Sobek on the other. It forms the major steep cliff from an edge (the Neith-Wosret boundary) down into the neck itself. The surface is very rough on intermediate scales. There do not appear to be any large scale structures. Its surface appearance seems uniform. Hence, no sub-regions are proposed here.

Sobek is a long thin region running along the bottom of the "valley" between the head and the body. Its surface appearance is completely different to that of Hapi in the northern hemisphere. One end of Sobek (the Anuket end) is characterized by a series of steps (small cliffs) that are roughly orthogonal to the long axis of the neck (Fig. 17). These steps have been observed to be a source of small jet-like activity.

This stepped structure is confined to the Anuket end of Sobek and we define this as a sub-region (sub-region a). The transition to sub-region b comes from a small change in topography with sub-region b appearing to be at a slightly lower elevation. Across the boundary, the surface texture changes from larger small-scale roughness in sub-region a to a smoother

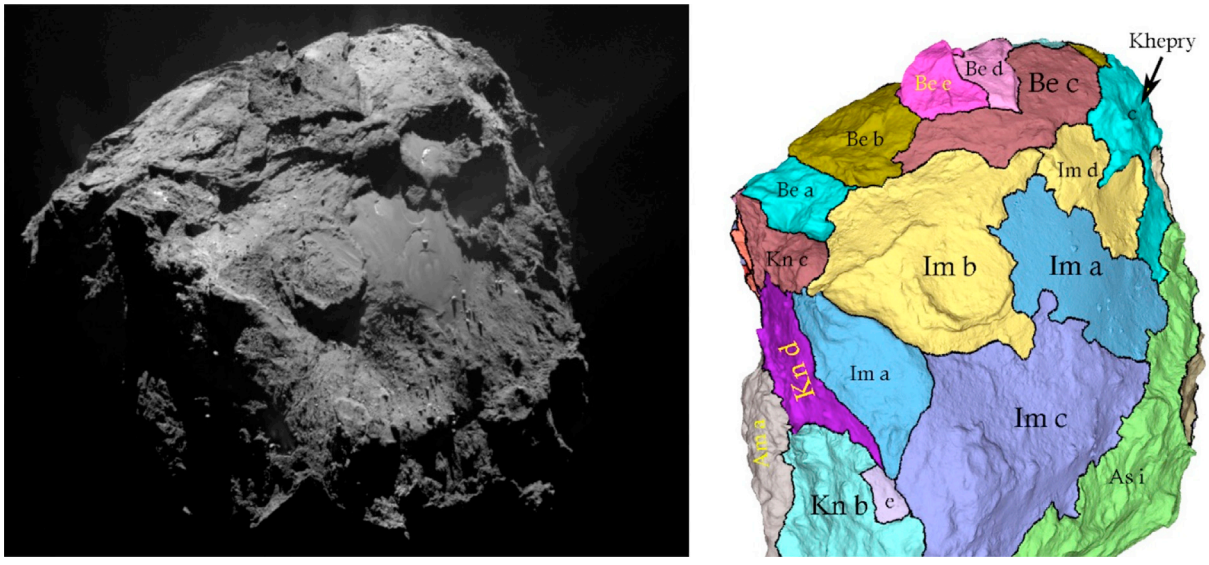

Fig. 16. The Bes and Imhotep sub-region definition. Left: OSIRIS image NAC_2015-08-01T23.55.10. Right: The 3D shape model. Bes mostly covers one long, thin face of the body of the nucleus with different topographical layers delinated by steep cliffs.

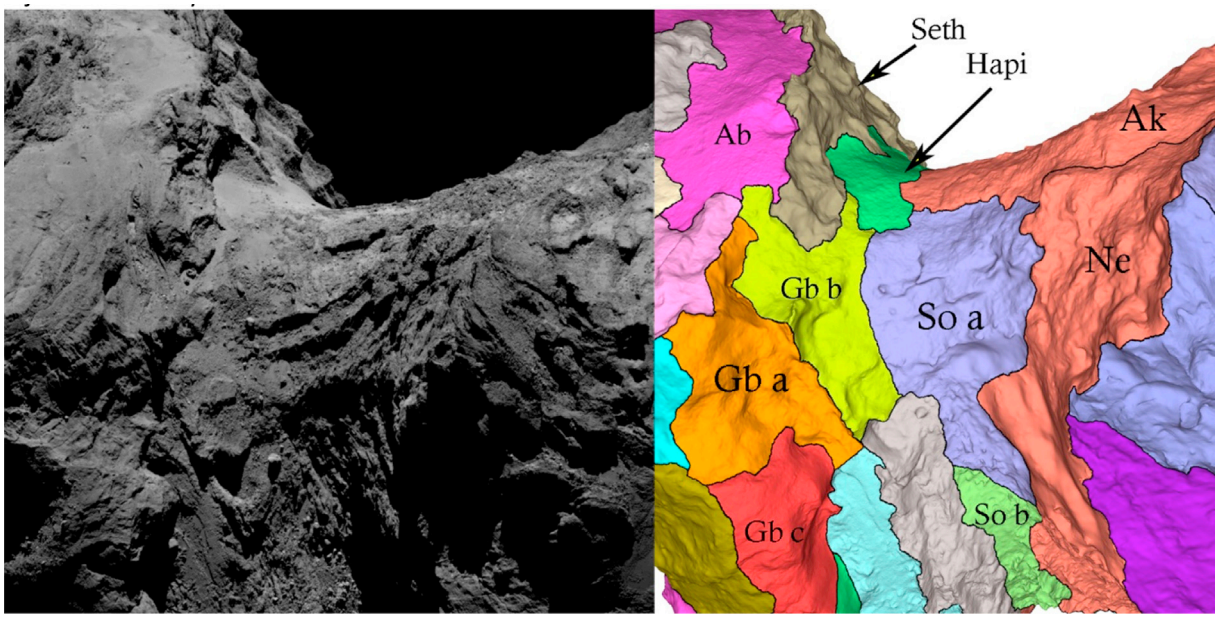

Fig. 17. Left: OSIRIS image NAC_2016-01-30T10.41.49.690Z_ID10_1397549900_F22. Right: The sub-region definition. The stepped structure of Sobek is evident at the centre of the image.

terrain. However, sub-region b is not completely smooth and at the Hapi-Bastet end of the region there are a significant number of knobs and small cliffs – particularly at the interface to Neith.

2.2.3. Head

2.2.3.1. Wosret (Wr). Wosret is a fascinating region. It gives the appearance of being a flat face on the southern side of the head of the nucleus. However, the shape model shows that this is not entirely accurate and the topographic and textural difference across the region can be clearly seen in suitable OSIRIS images (Fig. 18).

Sub-region a is defined as a flat, smooth surface. It does contain a long, narrow intrusion that seems to have different reflectance properties but this has been ignored here. Sub-region b is heavily fractured and it can be seen in Fig. 18 that it is not planar with sub-region a. This is very evident in the shape model and the boundary has been defined along the line where the change in slope occurs. This line is not cliff-like but fairly straightforward to see in the shape model.

Sub-region c is defined according to the change in texture. This change is easily seen in Fig. 18 and comes from greater intermediate scale roughness. This roughness is evident as a combination of quasi-circular depressions (pits) combined with non-aligned ridges.

2.2.3.2. Hatmehit (Hm). Hatmehit was one of the places on the nucleus to give a clear impression of being a single unit when the spacecraft arrived at the comet. The circular appearance of the whole structure is very striking. However, in detail, the structure is not symmetric and we split the structure into 3 sub-regions to reflect this (Fig. 19).

Sub-region a is the smooth almost circular surface area in the centre of the region. This straightforward definition has an advantage in that,

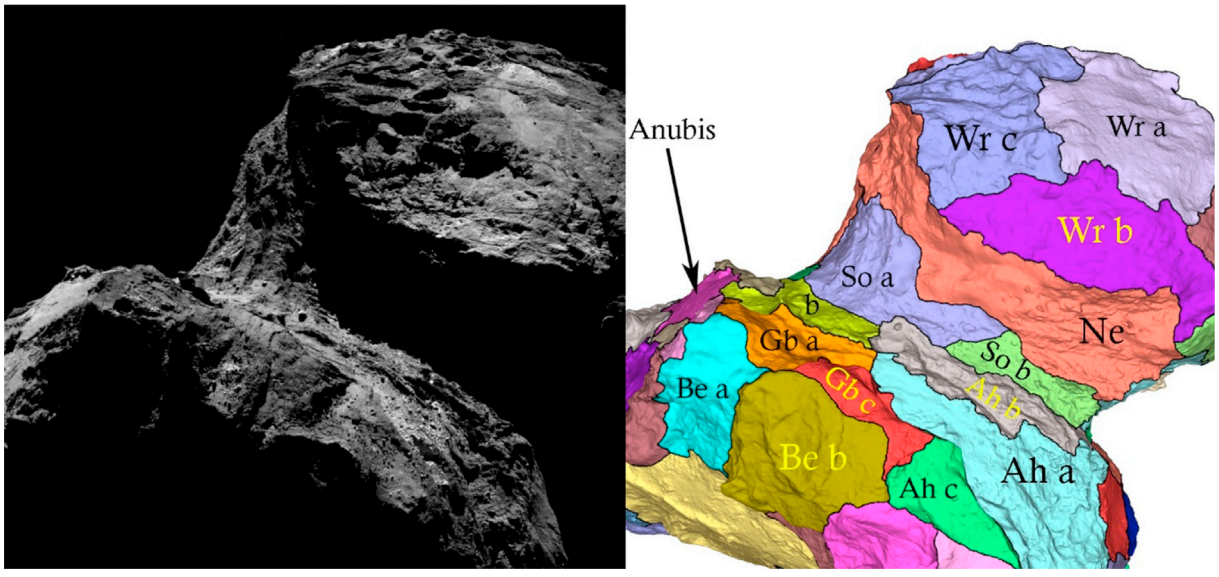

Fig. 18. Left: OSIRIS image NAC_2016-01-02T17.23.24.646Z_ID10_1397549300_F22. Right: The sub-region definition. The Wosret region is particularly interesting in this image. The image shows the topographic and textural differences that have led to the definition of 3 sub-regions.

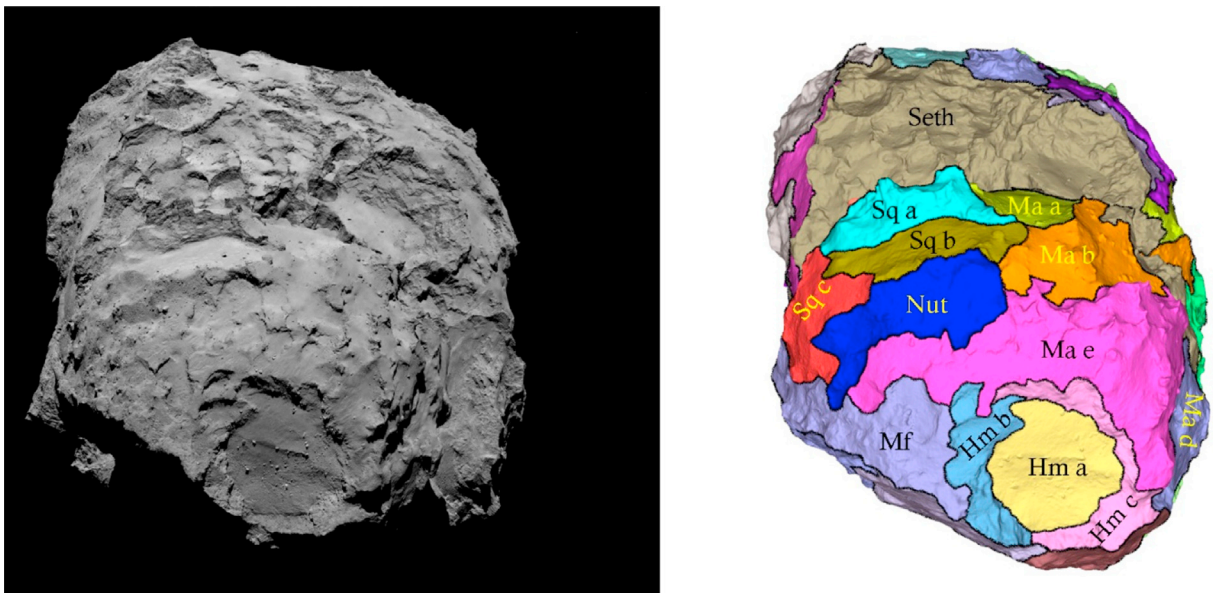

Fig. 19. Left: OSIRIS image NAC_2014-08-06T01.19.14. Right: The sub-region definition showing the nucleus along its long access with Hatmehit in the foreground.

while it is widely assumed that the Hatmehit interior has been produced by the same process that produced the rim, a relationship has not actually been proven. Production via an impact phenomenon of some sort might be a hypothesis but it must explain the flat nature of the interior and the differences between the two sides of the rim.

Sub-region a has a small change in slope passing through its centre. However, there seems to be no other textural change associated with this. The presence of talus and dust cover prevents any further sub-division.

Sub-region b abuts Wosret and Maftet. This sub-region shows a transition to the Maftet-like surface. The gain in elevation from sub-region a to the Maftet boundary is gradual. Within this, there are arcuate depressions. In sub-region c, on the other hand, the transition to Bastet and Ma'at is much steeper. The surface is rock-like and heavily fractured in places. There are steep cliffs that are arcuate near the interface with Maat and some evidence of layering (Giacomini et al., 2016).

2.2.3.3. Serqet (Sq) and Nut (Nu). Serqet is a remarkable region and we have sub-divided it into 3 sub-regions. The most remarkable aspect is that the surface changes from a smooth, dust covered, horizontal plane to an almost vertical rock-like structure at a very distinct boundary. The sub-region definition separates these two areas (Fig. 20).

In the original regional definition, Serqet was extended to meet Maftet. The coverage of this area at the time was rather poor. The shape model shows there is a rapid change of slope between sub-regions a and b and the rest of Serqet. Hence, we define this transitional surface as being sub-region c. This evidence for some quasi-circular and arcuate depressions in sub-region c suggests that the substrate has some similarity to the adjacent Maftet region.

The shape model confirms the impression given in the first data that Nut is a depression distinct from Serqet and the Ma'at region on its opposite side. The shape model shows that the change in slope at the

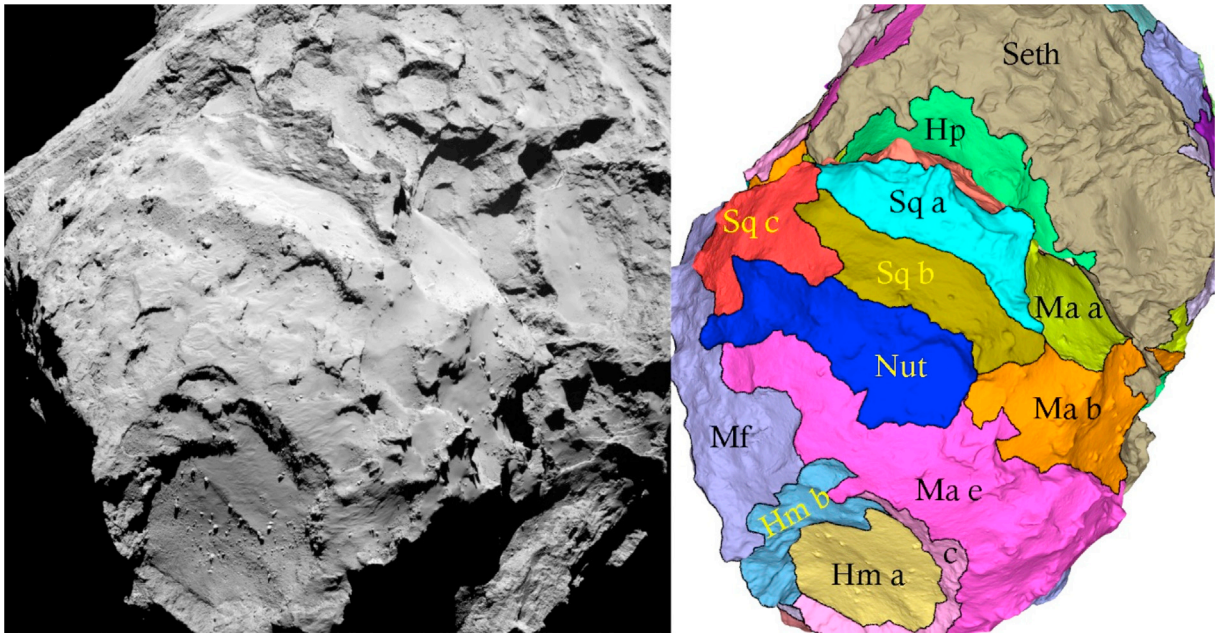

Fig. 20. Left: OSIRIS image NAC_2015-03-05T00.38.41.069Z_ID10_1397549003_F41. Right: The sub-region definition showing Serqet in the centre of the image. Ma'at sub-regions a and b are also evident to the right of Serqet. The Hatmehit sub-regions (a, b, and c) are also marked.

boundary to Serqet sub-region b is similar to that seen at the sub-region a to b boundary although 2D images alone completely fail to give this impression. There does not seem to be any justifiable reason to sub-divide Nut.

2.2.3.4. Ma'at (Ma). Like Ash on the body of the nucleus, Ma'at was defined through the dust coverage on north-facing surfaces. We take the same approach with Ma'at as taken with Ash and look at topographic differences and evidence of non-uniformity in the substrate to define sub-regions. The process has resulted in 5 distinct sub-regions (Fig. 21).

Sub-region a is a smooth, shallow depression with numerous knobs. It adjoins Anuket and Serqet. A ridge separates sub-region a from sub-region b which also adjoins Serqet. The surface of b is similar but contains an irregular structure close to its centre. In this region, there are numerous knobs visible that are probably the topographic expressions of the substrate through the dust covering.

Sub-region c contains a number of quasi-circular pits that have been shown to be active. There are several arcuate depressions superposed on a substrate that seems to have significant large scale roughness. Its topographic appearance is similar to parts of Seth and one of the Ash sub-regions.

Sub-region d is a plateau and more planar than the rest of the region. It is bounded by an abrupt, sharp change in slope at its boundary with Bastet. The boundary with sub-region e is a cliff of intermediate slope. A knobbly ridge is present near its centre.

Sub-region e covers the rest of Ma'at. It is dust-covered but the substrate is obviously rough on large scales. It becomes smoother towards the boundary with Nut but this is gradual.

2.2.3.5. Bastet (Bs). The boundaries between Bastet, Hathor and Wosret were poorly observed during the early phase of the mission and good observations were only obtained as the comet reached equinox inbound.

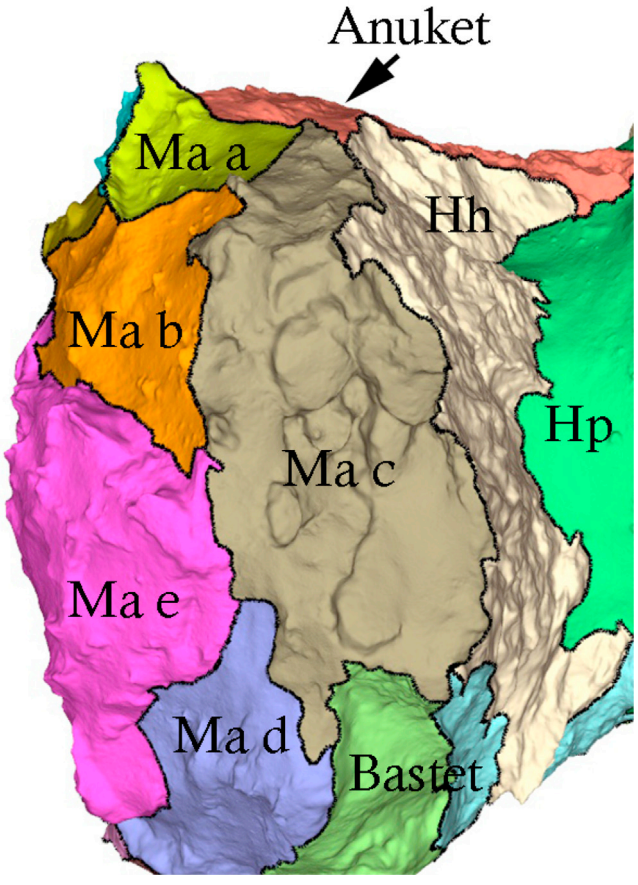

Fig. 21. The shape model showing the 5 sub-regions of Maat. Note the different surface appearances.

A single really good view of the Bastet region is not straightforward because the region has been defined as going from the Wosret (south-facing) region to the Hathor region on the opposite of the head. The region appears to have 3 components. The sub-region adjoining Wosret is undulating but with small scale roughness and little or no deposited dust. The border with Wosret is mostly defined through a small scarp.

Sub-region b is defined at a sharp change in the surface plane as the region wraps around the head. This sub-region has a U-shaped depression and has more large-scale roughness than sub-region a.

Sub-region c has significant intermediate scale roughness and is possibly a transition region between the smoother terrains of sub-regions a and b and the fractured, rocky appearance associated with the ~900 m high cliff dominated, Hathor. Sub-region c is not planar with Hathor. Its extent down into the neck is not easily determined. In this part of the sub-region, there is similarity in surface appearance to both the Neith region and part of Sobek sub-region b. This leads to some ambiguity.

2.2.3.6. Anuket (Ak), Hathor (Hh) and Maftet (Mf). The improvements in the shape model do not suggest the need for sub-division of these regions. Hathor is dominated by the 900 m high cliff that drops from the Ma'at region on the head to the Hapi region in the neck. The roughness and the appearance of the cliff may not be perfectly uniform across its surface but there are certainly no obvious differences that would suggest a major advantage in sub-dividing the region.

Similarly Anuket is fairly uniform in appearance being mostly smooth at intermediate and large scales but with small scale roughness giving a rocky appearance. The boundary with Neith is gradual but the boundaries with Serqet, Hathor and Hapi are extremely clear.

Maftet is dominated by quasi-circular and elliptical depressions with a significant dust covering. There are gradual transitions towards Hatmehit and Serqet but there do not appear to be any intermediate scale differences in the surface properties (either structurally or topographically) to require sub-division.

3. Derived products

3.1. Surface areas

The total surface area of the nucleus with this model is 51.74 km^2 (Preusker et al., 2017). The derived surface regions and sub-regions can be used to determine some values of interest. It should be noted that we use the following only as examples of the way in which the surface areas derived here might be used.

3.1.1. Airfall deposits

Ma'at, Ash, and Babi are regions that are mostly dust-covered probably as a result of transport/sedimentation of dust (Thomas et al., 2015a, b). They are pre-dominantly in the northern hemisphere. The dust covering is associated with non-escaping particles emitted from the Hapi region and the southern hemisphere (Thomas et al., 2015a,b; Keller et al., 2017). The total area of the three regions is 11.53 km^2 or 22.3% of the total surface. There are sub-regions that appear less covered or devoid of these deposits. Excluding these from the calculation gives 9.43 km^2 (18.2%). Seth has several north-facing probably dust-covered surfaces but these would have to be included individually in any calculation as there are numerous vertical surfaces within the region that contribute to the total area. We note that some authors may choose to assume that the surfaces of parts of Imhotep, Serqet, Maftet, and Anubis are also influenced by sedimenting dust.

3.1.2. Smooth (changing) surfaces

The regions of Anubis, Hapi and parts of Imhotep (sub-regions a and d) are smooth and inferred to be dust covered. They also exhibit surface

changes that are inferred to be related to activity (El-Maarry et al., 2016) following the appearance of quasi-elliptical depressions. The surface area of these regions and sub-regions is 4.49 km^2 (8.7%). Serqet sub-region b also appears to be dust-covered and smooth. However, no evidence for quasi-elliptical depressions has yet been presented for Serqet.

3.1.3. Fractured cliffs on the head

The head of the nucleus has three main regions that are almost orthogonal to local gravity and comprise fractured or rough terrain leading down into the base of the neck. These regions are Neith, Hathor, and part of Bastet (sub-region c). These regions comprise 8.3% of the surface area of the nucleus. Anuket is the only other region which drops to the neck on the head side of the nucleus. However, the surface of Anuket, which has a surface area = 4.0% of the whole nucleus, is more consolidated.

3.1.4. Regions with pits

The presence of active pits on the nucleus was one of the more remarkable results from the observations of the nucleus. Activity was observed from pits in the Seth and Ma'at regions (Vincent et al., 2015) specifically. In Ma'at, the pitted structures are restricted to sub-region c in our definition. Furthermore, structures looking very similar to those seen in Seth are apparent in Ash sub-region g (see also Ip et al., 2016). These three sub-regions alone contribute 11.6% of the surface area (although ¾ of that area is solely Seth's contribution). Some parts of Atum also show some quasi-circular structures that might be related and isolated pits are evident elsewhere. Fornasier et al. (2017) noted the presence of an active pit in Anhur. Hence, around 11–15% of the surface area shows evidence of larger scale pits that were either active during the present perihelion passage or (by analogy) were active in the past.

3.1.5. Arcuate surfaces

Maftet shows a large number of arcuate depressions that are generally shallow compared to the pits seen in Seth or Ma'at. These structures are also seen in the rim of Hatmehit (sub-region b) and gradually disappear as one crosses the Serqet c transitional region. Including the whole of Serqet c, this results in a contribution to the surface area of 2.6%.

3.1.6. The Bes plateaux

The shape model shows the sub-regions b, d, and e of the Bes region having distinct scarps and suggest some form of large scale layering. The corresponding surface areas are 0.65 km^2, 0.32 km^2, and 0.34 km^2 respectively. The cliffs have been seen to be active and hence a volume estimate may provide some insight into the available volume of source material. The plateaux sit topographically on top of Bes sub-region c on the equatorial side of the nucleus and the material exposed as the steep cliffs of Geb (sub-regions a and c) and Anhur (sub-region c). Although these cliffs seem very prominent in the 3D shape model, the total surface area of these 3 sub-regions only covers 1.9% of the nucleus.

3.2. Morphological roughness

3.2.1. Regional

The definition of the roughness of a non-planar (3D) surface is not trivial. Issues include the scale length over which the roughness is computed and whether the large-scale curvature of the body is removed and how that is actually performed. This problem is one encountered in the computer graphics industry. For this work, we look at the relative roughness between regions using a technique developed by Lavoué (2009) for this purpose. The reader is referred to Lavoué (2009) for details but we give a brief summary of the key points of the algorithm.

In this algorithm, for each vertex of the shape model, the curvature tensor is calculated and then the principal curvature values (k_{min}, k_{max}) are extracted. These correspond to the eigenvalues of the curvature tensor. For the roughness estimation algorithm, the maximum curvature k_{max}, is determined since this value reflects the bumpiness of the surface.

The roughness measure of Lavoué is then based on a scale parameter which determines the frequencies that have to be considered as roughness. In order to establish this scale parameter, a local window of a mesh is defined. Although the concept of a local window is trivial in 2D image, it becomes significantly more complex for 3D objects on an irregular mesh. Lavoué defines the local window of a single vertex by using a sphere of definable radius and determining where this sphere intersects with the mesh. The algorithm is then based on the average curvature difference between the original object and a smoothed version where the smoothing distance is linked to a scale parameter that is in turn linked to the radius of the local window. It is this step that allows determination of roughness over different scale lengths. It also eliminates resolution issues in studying facet-to-facet roughness. Facet-to-facet roughness suffers from resolution issues and the noise in the facet determination algorithm.

The approach is quantitative in the sense that a numerical value for the roughness can be extracted. However, the interpretation of the numerical result in terms of a slope distribution is not straightforward because the algorithm is effectively determining average curvature differences between the original object and a smoothed version of that object on a scale length given by the scale parameter. Hence, the algorithm is adequate for comparisons between regions on 67P and allows us to make statements about relative roughness differences with some level of confidence.

It should be noted that in the published algorithm, the scale of the roughness is expressed as percentage with respect to the size of a bounding box that surrounds the surface being investigated. This implies that regions that have different total sizes would be examined for roughness over different scale lengths. With the help of the author (Lavoué, pers. comm.), we have implemented a small modification so that roughness is characterized over a fixed distance irrespective of the total size of the region. We have used here 20 m as the roughness scale which is around 20 times larger than the quality of the SHAP7 model.

In Fig. 22, we show a plot of histograms of the roughness values for the Apis and Hapi regions. Both these regions are relatively flat and

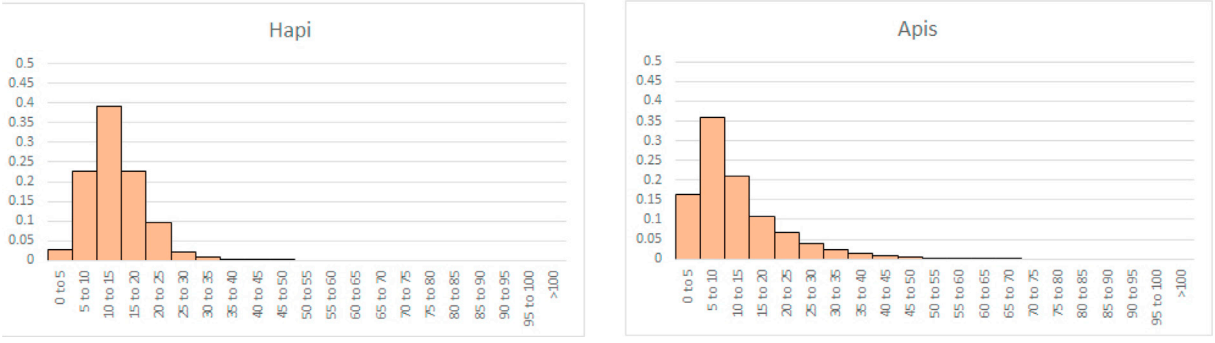

Fig. 22. A quantitative expression of the roughness of the Apis and Hapi regions on the nucleus. The y-axis expresses the normalized area in each bin. The x axis defines the effective curvature difference between the original object and a smoothed version of that object with a scale parameter equal to 20 m.

smooth over large areas and distances. The surface of Apis does not appear dust covered. The y-axis of the plot shows the areas of facets in each bin normalized to the total area of all facets in the region. The x-axis gives the bins and is given in curvature units, [1/km]. This follows the definition of Cauchy who defined the centre of curvature as the intersection point of two infinitely close normals to a curve, the radius of curvature as the distance from the point to the centre of curvature, and the curvature itself as the inverse of the radius of curvature thereby giving the expressed units. Clearly, the larger the value, the greater the roughness through lower radii of curvature.

The shape of the curve resembles a Maxwell-Boltzmann speed distribution but this is a coincidence and attempts to use this type of mathematical distribution as a fitting formula produce nonsensical results. Hence, we have merely fit the peak with a Gaussian and express the results as the position and width of that Gaussian in order to give two easily interpretable numerical values describing the distribution.

Fig. 22 should be compared to Fig. 23 which shows the same plot but for the Anhur and Sobek regions. The histograms are markedly different from the Apis and Hapi results. This indicates a quantitative difference in roughness between the Anhur-Sobek regions and the Apis-Hapi regions that agrees with their subjective appearance.

In Table 2, we take this a step further by computing the peak and the width (1/e width) of the distributions for each region. As stated above, a Gaussian fit has been used here to identify the peak although there is no doubt that the exact functional form of the distribution is significantly different from a Maxwellian. Nonetheless, we are simply trying to identify if the roughness measure gives numerical support to our subjective impression that some areas are rougher than others. It should be noted that the tail of the distribution influences the position of the Gaussian peak and so distributions with a long tail will produce positions of the maxima that are at higher values than the maximum probability. Through modifying the box size, we estimate the "error" in the values to be of the order of ±2 although this is a somewhat subjective value.

The results in Table 2 are quite informative. For example, it is confirmed that regions such as Khonsu, Atum, Sobek, and Hathor are indeed very rough with Sobek being quantitatively the roughest of these four. Anhur is rougher still. Bes is also rough despite the fact that its plateaux are well organized and layer-like. This might indicate an issue with the method where regions are defined with respect to layers with steep slopes.

The smoother regions include (apart from Hapi and Apis) Aker and Anubis as one might expect. Babi is, perhaps surprisingly, smooth in the peak roughness metric. However, it is noticeable that the width of the distribution for Babi is considerably broader than for the other smooth terrains. This may reflect the fact that Babi has two distinctly different types of terrain that we have separated into two sub-regions. Although both sub-regions are dust covered, Babi a has significant large scale roughness while Babi b is much smoother.

Both Anuket and Imhotep give the visual impression that they are fairly smooth but, in both cases, the roughness parameter suggests these surfaces are rougher than, for example, Maftet or Bastet, respectively. In the case of Anuket, the surface is rather uniform in visual appearance and this is substantiated by the lower value for the width of the distribution when compared to regions with a similar peak roughness parameter. Imhotep is far more diverse in surface morphology which has resulted in our defining 4 sub-regions. However, the width of the distribution is actually less than the value for Anuket. This leads to the conclusion that while these statistics are broadly following our perception and giving numerical confidence to our interpretation of surface roughness differences, blindly accepting the numerical results might lead to misinterpretation in certain specific cases.

Table 2
The roughness parameters for each region giving the peak bin and the width of the distribution.

Region	Peak roughness parameter	Width of roughness distributions
Hapi	8.36	5.31
Anubis	11.63	4.36
Geb	12.27	6.9
Babi	12.6	11.91
Apis	12.77	5.03
Ma'at	12.99	10.43
Hatmehit	13.79	7.45
Aker	14.1	6.44
Serqet	14.13	7.69
Nut	14.33	6.72
Bastet	14.76	7.27
Imhotep	15.14	7.22
Khepry	15.71	6.89
Ash	15.74	9.45
Seth	16.16	12.65
Aten	16.75	12.1
Maftet	16.92	8.61
Anuket	17.01	7.83
Atum	17.09	8.69
Bes	17.15	8.17
Wosret	18.26	8.59
Neith	18.63	15.1
Khonsu	18.83	8.46
Hathor	19.6	8.66
Sobek	21.4	9.85
Anhur	24.47	13.96

3.2.2. Sub-regional

The computation of the roughness parameters has also been made for the 71 sub-regions identified in Table 1 and we look at some specific examples.

Imhotep has four sub-regions with sub-region a being very smooth and a site where surface changes were observed. In Table 3, we show the peak of the roughness distribution function for the four individual sub-regions of Imhotep and sub-regions of note elsewhere. As expected, the smoothest sub-region of Imhotep has the lowest roughness parameter with a value of below 10 and only slightly higher than that of Hapi. Sub-

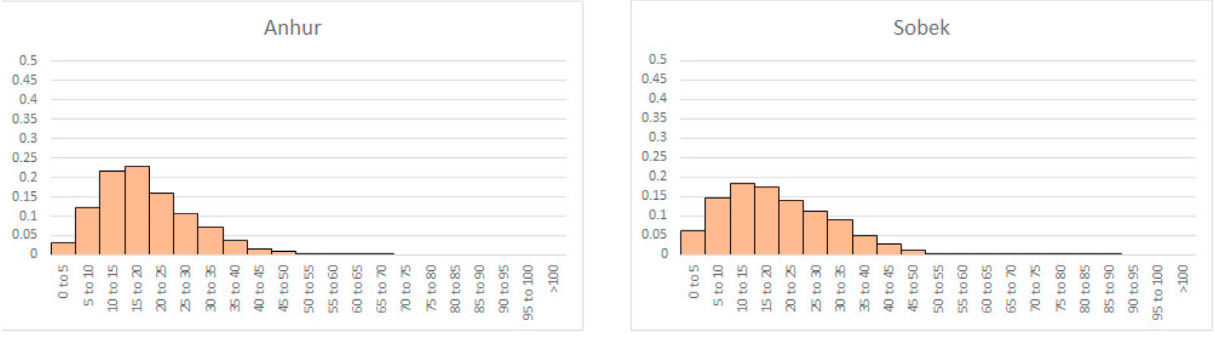

Fig. 23. As Fig. 22 but for the Anhur and Sobek regions. Notice that the distribution is much broader indicating a large distribution of roughness. The peak of the distribution is also shifted to higher roughness values.

Table 3
Peak roughness parameter for the individual sub-regions within some regions.

Region	Sub-region	Peak roughness parameter
Imhotep	a	9.58
	b	16.7
	c	17.52
	d	12.78
Hatmehit	a	10.36
	b	16.14
	c	17.91
Serqet	a	18.8
	b	11.96
	c	13.7
Babi	a	16.61
	b	9.59
Anhur	a	27.06
	b	25.53
	c	7.28

region d, which also showed evidence of changes and dust coverage is shown to be rougher (presumably arising from the depression rims surrounding the dust deposit) while sub-regions b and, particularly, c are indicated as being much rougher although not as rough as Sobek, Anhur (sub-regions a and b), or Neith. This result confirms quantitatively the visual perception.

Hatmehit shows a similar result. The central dusty sub-region (sub-region a) has a roughness parameter comparable to but slightly higher than that of Imhotep sub-region a. The rim of the "crater" is appreciably rougher with the arcuate sub-region (b) being slightly less rough than the cliff-like sub-region.

Serqet has a cliff (sub-region a) and a dusty, relatively smooth sub-region at the base of the cliff (sub-region b). Table 3 again indicates quantitative agreement with the perception.

Babi was referred to above as having a broad distribution and indeed the two sub-regions that have been defined have very different roughness parameters. Sub-region b has a value of 9.59 (a value seen for smooth sub-regions) while the value for sub-region a is 16.61 placing this sub-region at a roughness level similar to rougher areas of Ash. Here again, the perception of significant variation within the region is confirmed and a difference between the defined sub-regions is apparent.

For Wosret, the very rough pitted terrain of sub-region c is also identified in the analysis as being very rough (24.49) with the flatter face (sub-region a) being clearly smoother (13.58). The fractured terrain towards the neck is intermediate.

The roughest sub-region is Sobek sub-region b (31.78) while the smoothest is (perhaps surprisingly) Geb sub-region c (6.90). The latter forms part of the steep cliff leading up to the Bes region and is completely devoid of boulders. The width of the distribution is however quite large (10.41). By comparison, the Imhotep smooth sub-region (sub-region a) has a distribution width of only 3.30 indicating greater uniformity as is apparent in the images. It is to be noted that Anhur sub-region c, which adjoins Geb sub-region c has a similar low value of the roughness parameter (7.28 and the second lowest value of all sub-regions). This suggests that Anhur sub-region c might have been better defined as part of Geb.

4. Summary and conclusions

The definitions of regions on the nucleus that were originally made on 2D images (Thomas et al., 2015a,b; El-Maarry et al., 2016, El-Maarry et al., 2017a,b) can be mapped back onto the shape model of the nucleus (SHAP7; Preusker et al., 2017) to provide a self-consistent definition in three dimensions. The accuracy of the SHAP7 model (metre-scale) and the use of 3D tools have allowed us to ensure that the regional definition is complete. Detailed study of the shape model in combination with 2D images indicates that many regions can be further sub-divided into sub-regions of common morphology. This is particularly true in regions that had been only poorly imaged at the time of the original regional definition – notably the neck of the nucleus in the southern hemisphere. We provide a comprehensive table of these sub-regions and have mapped them onto the 3D shape model. Detailed comparisons between the sub-region definitions and 2D images acquired by OSIRIS have been presented to justify our interpretation and definition.

We have illustrated the use of the surface areas to compute the total surface areas of morphological types on the nucleus.

We have used the SHAP7 model and the regional definition to compute a quantitative measure of surface roughness for each region. The algorithm has been proposed for computer graphics applications (Lavoué, 2009) and gives a measure for the roughness that broadly agrees with our perception of the roughness from visual (2D) images and the appearance of the shape model. The algorithm identifies Sobek and Anhur as the roughest regions on the nucleus while Hapi (unsurprisingly) and the flat-faced rocky surface of Apis are the least rough on regional scales. When running the algorithm on the sub-region definition, results consistent with our separation of different terrain types into sub-regions can be found. In particular, the sub-region definitions of Imhotep, Babi and Wosret appear to be well justified. While this algorithm has some drawbacks, particularly the absence of a clear physical relationship to the derived parameters, the relative ordering of regions and sub-regions with respect to their roughness parameters appears to have potential for helping define surface units with common properties.

Acknowledgements

The team from the University of Bern is supported through the Swiss National Science Foundation and through the NCCR PlanetS. The project has also received funding from the European Union's Horizon 2020 research and innovation programme under grant agreement No 686709. This work was supported by the Swiss State Secretariat for Education, Research and Innovation (SERI) under contract number 16.0008-2. The opinions expressed and arguments employed herein do not necessarily reflect the official views of the Swiss Government.OSIRIS was built by a consortium led by the Max-Planck-Institut für Sonnensystemforschung, Göttingen, Germany, in collaboration with CISAS, University of Padova, Italy, the Laboratoire d'Astrophysique de Marseille, France, the Instituto de Astrofísica de Andalucia, CSIC, Granada, Spain, the Scientific Support Office of the European Space Agency, Noordwijk, The Netherlands, the Instituto Nacional de Técnica Aeroespacial, Madrid, Spain, the Universidad Politéchnica de Madrid, Spain, the Department of Physics and Astronomy of Uppsala University, Sweden, and the Institut für Datentechnik und Kommunikationsnetze der Technischen Universität Braunschweig, Germany.

Appendix A. Supplementary data

Supplementary data related to this article can be found at https://doi.org/10.1016/j.pss.2018.05.019.

References

El-Maarry, M.R., 53 colleagues, 2015. Regional surface morphology of comet 67P/Churyumov-Gerasimenko from Rosetta/OSIRIS images. Astron. Astrophys. 583 https://doi.org/10.1051/0004-6361/201525723. A26.

El-Maarry, M.R., 51 colleagues, 2016. Regional surface morphology of comet 67P/Churyumov-Gerasimenko from Rosetta/OSIRIS images: the southern hemisphere. Astron. Astrophys. 593. A110.

El-Maarry, M.R., 51 colleagues, 2017a. Regional surface morphology of comet 67P/Churyumov-Gerasimenko from Rosetta/OSIRIS images: the southern hemisphere (Corrigendum). Astron. Astrophys. 598. C2.

El-Maarry, M.R., 55 colleagues, 2017b. Surface changes on comet 67P/Churyumov-Gerasimenko suggest a more active past. Science 355, 1392–1395.

Fornasier, S., 53 colleagues, 2017. The highly active Anhur-Bes regions in the 67P/Churyumov-Gerasimenko comet: results from OSIRIS/ROSETTA observations. Mon. Not. Roy. Astron. Soc. 469, S93–S107.

Giacomini, L., et al., 2016. Geologic mapping of the Comet 67P/Churyumov-Gerasimenko's Northern hemisphere. Mon. Not. Roy. Astron. Soc. Lett. 462, S352–S367.

Ip, W.-H., et al., 2016. Physical properties and dynamical relation of the circular depressions on comet 67P/Churyumov-Gerasimenko. Astron. Astrophys. 591. A132.

Jorda, L., Gaskell, R., Capanna, C., Hviid, S., Lamy, P., Durech, J., Faury, G., Groussin, O., Gutiérrez, P., Jackman, C., Keihm, S.J., Keller, H.U., Knollenberg, J., Kuehrt, E., Marchi, S., Mottola, S., Palmer, E., Schloerb, F.P., Sierks, H., Vincent, J.-B., A'Hearn, M.F., Barbieri, C., Rodrigo, R., Koschny, D., Rickman, H., Barucci, M.A., Bertaux, J.L., Bertini, I., Cremonese, G., Da Deppo, V., Davidsson, B., Debei, S., De Cecco, M., Fornasier, S., Fulle, M., Guettler, C., Ip, W.-H., Kramm, J.R., Kueppers, M., Lara, L.M., Lazzarin, M., Lopez Moreno, J.J., Marzari, F., Naletto, G., Oklay, N., Thomas, N., Tubiana, C., Wenzel, K.-P., 2016. The global shape, density and rotation of Comet 67P/Churyumov-Gerasimenko from preperihelion Rosetta/OSIRIS observations. Icarus 277, 257–278.

Keller, H.U., Mottola, S., Hviid, S.F., Agarwal, J., Kührt, E., Skorov, Y., Otto, K., Vincent, J.-B., Oklay, N., Schröder, S.E., Davidsson, B., Pajola, M., Shi, X., Bodewits, D., Toth, I., Preusker, F., Scholten, F., Sierks, H., Barbieri, C., Lamy, P., Rodrigo, R., Koschny, D., Rickman, H., A'Hearn, M.F., Barucci, M.A., Bertaux, J.-L., Bertini, I., Cremonese, G., Da Deppo, V., Debei, S., De Cecco, M., Deller, J., Fornasier, S., Fulle, M., Groussin, O., Gutiérrez, P.J., Güttler, C., Hofmann, M., Ip, W.-H., Jorda, L., Knollenberg, J., Kramm, J.R., Küppers, M., Lara, L.-M., Lazzarin, M., Lopez-Moreno, J.J., Marzari, F., Naletto, G., Tubiana, C., Thomas, N., 2017. Seasonal mass transfer on the nucleus of comet 67P/Chuyumov-Gerasimenko. Mon. Not. Roy. Astron. Soc. 469, S357–S371.

Lavoué, G., 2009. A local roughness measure for 3D meshes and its application to visual masking. Trans. Appl. Percept. 5 (4), 21:1–21:23.

Preusker, F., Scholten, F., Matz, K.-D., Roatsch, T., Willner, K., Hviid, S.F., Knollenberg, J., Jorda, L., Gutiérrez, P.J., ühart, E.K., Mottola, S., A'Hearn, M.F., Thomas, N., Sierks, H., Barbieri, C., Lamy, P., Rodrigo, R., Koschny, D., Rickman, H., Keller, H.U., Agarwal, J., Barucci, M.A., Bertaux, J.-L., Bertini, I., Cremonese, G., Da Deppo, V., Davidsson, B., Debei, S., De Cecco, M., Fornasier, S., Fulle, M., Groussin, O., Güttler, C., Ip, W.-H., Kramm, J.R., K üppers, M., Lara, L.M., Lazzarin, M., Lopez-Moreno, J.J., Marzari, F., Michalik, H., Naletto, G., Oklay, N., Tubiana, C., Vincent, J.-B., 2015. Shape model, reference system definition, and cartographic mapping standards for comet 67P/Churyumov-Gerasimenko - stereo-photogrammetric analysis of Rosetta/OSIRIS image data. Astron. Astrophys. 583. A33.

Preusker, F., Scholten, F., Matz, K.-D., Roatsch, T., Hviid, S.F., Mottola, S., Knollenberg, J., Kührt, E., Pajola, M., Oklay, N., Vincent, J.-B., Davidsson, B., A'Hearn, M.F., Agarwal, J., Barbieri, C., Barucci, M.A., Bertaux, J.-L., Bertini, I., Cremonese, G., Da Deppo, V., Debei, S., De Cecco, M., Fornasier, S., Fulle, M., Groussin, O., Gutiérrez, P.J., Güttler, C., Ip, W.-H., Jorda, L., Keller, H.U., Koschny, D., Kramm, J.R., Küppers, M., Lamy, P., Lara, L.M., Lazzarin, M., Lopez Moreno, J.J., Marzari, F., Massironi, M., Naletto, G., Rickman, H., Rodrigo, R., Sierks, H., Thomas, N., Tubiana, C., 2017. Astron. Astrophys. 607 https://doi.org/10.1051/0004-6361/201731798. L1.

Sierks, H., Barbieri, C., Lamy, P.L., Rodrigo, R., Koschny, D., Rickman, H., Keller, H.U., Agarwal, J., A'Hearn, M.F., Angrilli, F., Auger, A.-T., Barucci, M.A., Bertaux, J.-L., Bertini, I., Besse, S., Bodewits, D., Capanna, C., Cremonese, G., Da Deppo, V., Davidsson, B., Debei, S., De Cecco, M., Ferri, F., Fornasier, S., Fulle, M., Gaskell, R., Giacomini, L., Groussin, O., Gutierrez-Marques, P., Gutiérrez, P.J., Güttler, C., Hoekzema, N., Hviid, S.F., Ip, W.-H., Jorda, L., Knollenberg, J., Kovacs, G., Kramm, J.-R., Kührt, E., Küppers, M., La Forgia, F., Lara, L.M., Lazzarin, M., Leyrat, C., Lopez Moreno, J.J., Magrin, S., Marchi, S., Marzari, F., Massironi, M., Michalik, H., Moissl, R., Mottola, S., Naletto, G., Oklay, N., Pajola, M., Pertile, M., Preusker, F., Sabau, L., Scholten, F., Snodgrass, C., Thomas, N., Tubiana, C., Vincent, J.-B., Wenzel, K.-P., Zaccariotto, M., Pätzold, M., 2015. On the nucleus structure and activity of comet 67P/Churyumov-Gerasimenko. Science 347 aaa1044, 23 January 2015.

Thomas, N., Sierks, H., Barbieri, C., Lamy, P.L., Rodrigo, R., Rickman, H., Koschny, D., Keller, H.U., Agarwal, J., A'Hearn, M.F., Angrilli, F., Auger, A.-T., Barucci, M.A., Bertaux, J.-L., Bertini, I., Besse, S., Bodewits, D., Cremonese, G., Da Deppo, V., Davidsson, B., De Cecco, M., Debei, S., El-Maarry, M.-R., Ferri, F., Fornasier, S., Fulle, M., Giacomini, L., Groussin, O., Gutierrez, P.J., Güttler, C., Hviid, S.F., Ip, W.-H., Jorda, L., Knollenberg, J., Kramm, J.-R., Kührt, E., Küppers, M., La Forgia, F., Lara, L.M., Lazzarin, M., Lopez Moreno, J.J., Magrin, S., Marchi, S., Marzari, F., Massironi, M., Michalik, H., Moissl, R., Mottola, S., Naletto, G., Oklay, N., Pajola, M., Pommerol, A., Preusker, F., Sabau, L., Scholten, F., Snodgrass, C., Tubiana, C., Vincent, J.-B., Wenzel, K.-P., 2015a. The morphological diversity of comet 67P/Churyumov-Gerasimenko. Science 347 aaa0440, 23 January 2015.

Thomas, N., Davidsson, B., El-Maarry, M.R., Fornasier, S., Giacomini, L., Gracia Berna, A.G., Hviid, S.F., Ip, W.-H., Jorda, L., Keller, H.U., Knollenberg, J., Kührt, E., La Forgia, F., Lai, I.L., Liao, Y., Marschall, R., Massironi, M., Mottola, S., Pajola, M., Poch, O., Pommerol, A., Preusker, F., Scholten, F., Su, C.C., Wu, J.S., Vincent, J.-B., Sierks, H., Barbieri, C., Lamy, P.L., Rodrigo, R., Rickman, H., Koschny, D., A'Hearn, M.F., Barucci, M.A., Bertaux, J-L., Bertini, I., Cremonese, G., Da Deppo, V., Debei, S., Fulle, M., Groussin, O., Gutierrez, P.J., Kramm, J.-R., Küppers, M., Lara, L.M., Lazzarin, M., Lopez Moreno, J.J., Marzari, F., Michalik, H., Naletto, G., Güttler, C., 2015b. Redistribution of particles across the nucleus of comet 67P/Churyumov-Gerasimenko. Astron. Astrophys. 583 https://doi.org/10.1051/0004–6361/201526049. A17.

Vincent, J.-B., 66 colleagues, 2015. Large heterogeneities in comet 67P as revealed by active pits from sinkhole collapse. Nature 523, 63–66.

Vincent, J.-B., 54 colleagues, 2016. Are fractured cliffs the source of cometary dust jets? Insights from OSIRIS/Rosetta at 67P/Churyumov-Gerasimenko. Astron. Astrophys. 587. A14.